Electronic Supporting Information

Ferrocene-driven Single-Chain Polymer Compaction

Sebastian Gillhuber,[a,b,c] Joshua O. Holloway,[b,c] Hendrik Frisch,[b,c] Florian Feist,[d] Florian Weigend,[e] Christopher Barner-Kowollik*[b,c,d] and Peter W. Roesky*[a]

[a] Institute of Inorganic Chemistry, Karlsruhe Institute of Technology (KIT), Engesserstraße 15, 76131 Karlsruhe, Germany, E-mail: roesky@kit.edu

[b] School of Chemistry and Physics, Queensland University of Technology (QUT), Brisbane 2 George Street, QLD 4000, Australia, E-mail: christopher.barnerkowollik@qut.edu.au

[c] Centre for Materials Science, Queensland University of Technology (QUT), Brisbane 2 George Street, QLD 4000, Australia

[d] Institute of Nanotechnology (INT), Karlsruhe Institute of Technology (KIT), Hermann-von-Helmholtz-Platz 1, 76344 Eggenstein-Leopoldshafen, Germany, E-mail: christopher.barner-kowollik@kit.edu

[e] Fachbereich Chemie, Philipps-Universität Marburg, Hans-Meerwein-Straße 4, 35043 Marburg, Germany

Table of Contents

1 Materials and Methods

Dichloro-(1,5-cyclooctadiene)-palladium(II) (36.7 % Pd, Alfa Aesar), dimethylanilinium tetrakis(pentafluorophenyl)borate (98 %, abcr), ferrocene (98 %, Merck), methanol (99.8 %, VWR Chemicals), *n*-butyllithium (1.6M or 2.5M in hexane, Thermo Fisher Scientific) and *n*-hexane (95 %, Merck) were used as received. Styrene (99.5 %, Thermo Fisher Scientific) and chloromethyl styrene (90 %, Thermo Fisher Scientific) were passed over a column of basic alumina (VWR) prior to polymerization.

2,2,6,6-Tetramethyl-1-(1-phenylethoxy)piperidine,[1] 2-ferrocenyl-1,10-phenanthroline[2] and 2,2-diphenyl-4-heptyn-1-amine[3] were prepared according to literature procedures.

Dichloromethane, diethyl ether and tetrahydrofuran were dried using an MBraun solvent purification system (SPS-800). Dichloromethane was additionally refluxed over phosphorus pentoxide and subsequently distilled under nitrogen atmosphere. *N,N*-Dimethylformamide was pre-dried over potassium hydroxide, then refluxed over phosphorous pentoxide, distilled, degassed and stored over molecular sieves. *N,N,N´,N´*-Tetramethylethylenediamine was pre-dried over potassium hydroxide, then refluxed over sodium hydride and subsequently distilled, degassed and stored over molecular sieves. Tetrahydrofuran-d_8 (99.5 % D, Eurisotop) and benzene-d_6 (99.5 % D, Eurisotop) were stored over Na/K alloy and distilled prior to use. Dry solvents were stored in Schlenk flasks or tubes with a J. Young valve under inert atmosphere.

All manipulations on air-sensitive compounds were performed under rigorous exclusion of oxygen and moisture under dry nitrogen using standard Schlenk techniques on a dual manifold Schlenk line, interfaced to a high vacuum (< 10^{-3} mbar) pump, or in an argon-filled MBraun glovebox.

2 Analytical Techniques

2.1 Nuclear Magnetic Resonance Spectroscopy

Nuclear magnetic resonance spectra were recorded on Bruker spectrometers (Avance Neo 400 MHz or Avance III 400 MHz) at 298 K, unless noted otherwise. The temperature was controlled using a Bruker Smart VT unit. ^{1}H chemical shifts were referenced internally using the residual solvent resonances and are reported relative to tetramethylsilane. Assignments were determined based on chemical shifts. As only NMR spectra of polymers are reported, the multiplicity of the resonances cannot be determined and is labelled as broad (br).

All DOSY experiments were performed at 298 K using a Bruker Avance III 400 MHz spectrometer, averaged diffusion coefficients are given in the experimental section. The Bruker pulse sequence *ledbpgp2s* using bipolar gradients with longitudinal eddy current delay and two spoil gradients was used. 32 gradient points were recorded in a linear manner ranging from 2 % to 98 % of the maximum applicable gradient strength. The gradient length (little delta) as well as the diffusion delay (big delta) were optimized prior to each DOSY measurement. The data was processed using TopSpin (Version 3.6.2) and Dynamics Center (Version 2.5.6). The assume constant offset option of Dynamics Center was used to obtain fits of adequate quality. The stacked DOSY NMR spectrum depicted in the main document was obtained with the Bayesian method within MestReNova (Version 14.1.2).

2.2 Size Exclusion Chromatography

Size exclusion chromatography measurements were conducted on a PSS SECurity^{2} system consisting of a PSS SECurity Degasser, PSS SECurity TCC6000 Column Oven (80 °C), PSS Gram Column Set (8x50 mm 10 µm Guard Column, 3 × 8x300 mm 10 µm Analytical Columns (30 Å, 2 × 1000 Å) and an Agilent 1260 Infinity II Isocratic Pump with seal wash (^{i}PrOH), Agilent 1260 Infinity II Standard Autosampler, Agilent 1260 Infinity II Diode Array and Multiple Wavelength Detector (A: 275 nm, B: 300 nm, C: 330 nm, D: 365 nm), Agilent 1260 Infinity II Refractive Index Detector (35 °C). HPLC grade DMAc with 0.1 w% LiBr (1.10 g·L^{-1}) was used as eluent at a flow rate of 1 mL·min^{-1}. Narrow disperse linear polystyrene (M_n: 266 g·mol^{-1} to 2.52 x 10^{6} g·mol^{-1}) (PSS ReadyCal) was used as calibrant. All samples were passed through 0.2 µm PTFE membrane filters prior to the measurements. Molar mass and dispersity analyses were performed with the PSS WinGPC UniChrom software (version 8.33).

2.3 Dynamic Light Scattering

Dynamic light scattering measurements were carried out on a Brookhaven Instruments NanoBrook Omni equipped with a 640 nm laser at 298 K. The polymer solutions were prepared by dissolving the samples in tetrahydrofuran at a concentration of approximately 5 mg·mL^{-1} and passing them through 0.2 µm PTFE membrane filters into 10 mm quartz cells. All measurements were conducted in backscattering mode with an angle of 173° relative to the incident

beam. The Particle Solutions software (Version 3.6.0.7122) was used. The dust rejection algorithm was applied. Given hydrodynamic diameters (D_h) were averaged over five consecutive measurements.

2.4 Energy Dispersive X-Ray Spectroscopy

Energy dispersive X-ray analysis was performed using an Ametec EDAX mounted on a Zeiss SEM Supra 35 VP scanning electron microscope. The powdered sample was fixed on a conductive carbon pad on an aluminum sample holder.

2.5 UV/Vis Spectroscopy

UV/Vis spectra were recorded on an Agilent Cary 5000 UV-VIS-NIR spectrophotometer. Measurements were performed at ambient temperature using a Helma Analytics quartz high precision cell (108-F-10-40) with a path length of 10 mm. The settings were: range 200-800 nm; interval: 1 nm; scan-rate: 300 $nm \cdot min^{-1}$; SBW = 2; double-beam mode; source changeover: 350 nm, zero and baseline scan. HPLC-grade dichloromethane was used for the measurements.

2.6 Liquid Chromatography Coupled Mass Spectrometry

Liquid Chromatography coupled Mass Spectroscopy (LC-MS) measurements were performed on an Agilent 1260 Infinity II system consisting of a quaternary pump (GB7111B), autosampler (G7129A, 100 µL sample loop), a temperature-controlled column oven (G7114A) and a variable UV-VIS detector (G7114 A, VWD, flow cell G7114A 018, d = 10 mm, V = 14 µL). Separation was performed on a C18 HPLC-column (Agilent Poroshell 120 EC-C18 4.6x100 mm, 2.7 µm) operating at 40 °C. A gradient of acetonitrile/water 10:90 – 80:20 v/v (additive 10 $mmol \cdot L^{-1}$ $NH_4CH_3CO_2$) at a flow rate of 1 $mL \cdot min^{-1}$ during 15 min was used as the eluting solvent. The flow was directed into an Agilent MSD (G6136BA, AP-ESI ion source). The instrument was calibrated in the m/z range 118-2121 in the positive mode and 113-2233 in the negative using a premixed calibration solution (Agilent). The following parameters were used: spray chamber flow: 12 $L \cdot min^{-1}$; drying gas temperature: 350 K, Capillary Voltage: 3000 V, Fragmentor Voltage: 100 V.

3 Synthetic Procedures

3.1 General Remarks

Equivalents referring to polymers given within the synthetic procedures were calculated under neglection of the influence of end groups, the chloromethylene moieties and SCNP crosslinking units on the molar mass. Hence, calculations are based on the molar mass of styrene alone.

The amount of chloromethyl styrene moieties in polymer **P1** was calculated according to:

$$\frac{N_{\mathrm{CMS}}}{N_{\mathrm{Styrene}} + N_{\mathrm{CMS}}} = \frac{5}{2\,\frac{Int(\mathrm{Ar,tot})}{Int(\mathrm{Benzyl})} + 1} = \frac{5}{2 * \frac{1.00}{0.06} + 1} = 0.14 \equiv 14\ \%$$

with:

N_{CMS}	Number of chloromethyl styrene moieties incorporated in the polymer chain
N_{Styrene}	Number of styrene moieties incorporated in the polymer chain
Int(Ar, tot)	Value of the integral obtained from integration of the aromatic region of the ^{1}H NMR spectrum of **P1** (δ = 7.40-6.26 ppm)
Int(Benzyl)	Value of the integral obtained from integration of the benzylic resonance of the ^{1}H NMR spectrum of **P1** (δ = 4.68-4.38 ppm)

The given equivalents of phenanthroline units within **2** are based on the assumption of quantitative conversion of the chloromethyl styrene moieties of precursor polymer **P1** when **2** is formed. The Pd equivalents given for **2-Pd** are based on the assumption of quantitative Pd functionalization of all phenanthroline moieties. The latter values must therefore be considered as upper limits for the actual amount of the respective functionalities.

3.2 Synthesis of Poly(styrene-*co*-chloromethyl styrene) (P1)

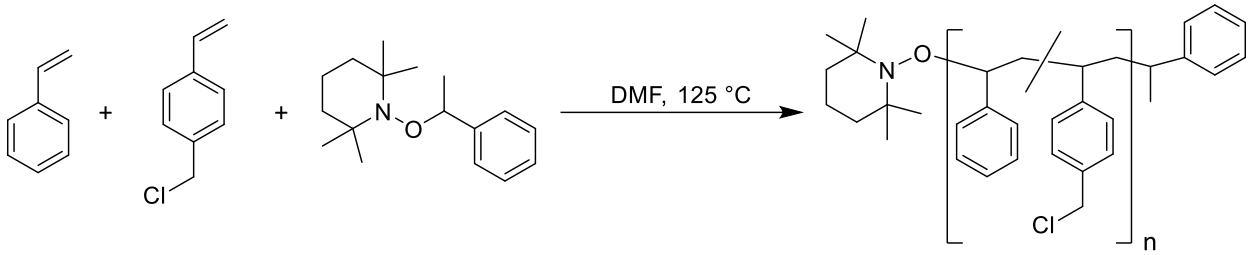

P1

46.6 mg of the NMP initiator 2,2,6,6-tetramethyl-1-(1-phenylethoxy)piperidine (0.178 mmol, 1.00 eq.) were dissolved in 4.20 mL of styrene (3.82 g, 36.9 mmol, 207 eq.) and 0.73 mL of chloromethyl styrene (0.788 g, 5.16 mmol, 28.9 eq.) and 2 mL DMF were added. The solution was degassed by three consecutive freeze-pump-thaw cycles and subsequently heated to 125 °C for 6 h. The reaction was stopped by cooling the flask with liquid nitrogen and opening it to air. THF was added and the polymer precipitated by dropwise addition of the solution to cold methanol. The precipitate was isolated by centrifugation and dried under reduced pressure to give **P1** as colorless solid (2.27 g).

^{1}H NMR (400 MHz, THF-d_8, 298 K): δ / ppm = 7.40-6.26 (br, aromatic), 4.68-4.38 (br, PhCH_2Cl), 2.37-1.22 (br, aliphatic backbone).

SEC (DMAc, RI, PS cal.): M_n = 16,300 g·mol^{-1}, M_p = 17,900 g·mol^{-1}, $Đ$= 1.15.

DLS (THF): D_h = 5.69 nm.

DOSY (400 MHz, THF-d_8, 298 K): D = 1.17·10^{-10} m^2·s^{-1}.

3.3 Synthesis of SCNP 1

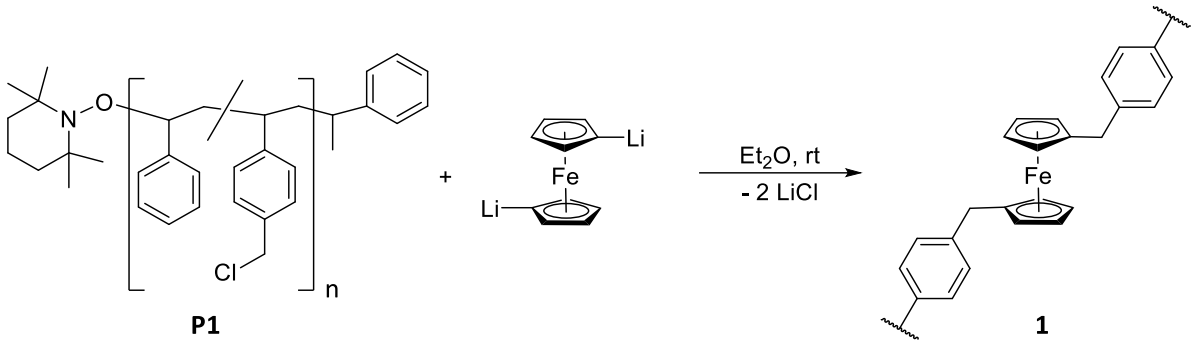

40.0 mg Ferrocene (0.215 mmol, 1.00 eq.) were dissolved in 4 mL of diethyl ether and 0.54 mL *n*-BuLi (1.6 M in hexane, 0.860 mmol, 4.00 eq.) and 0.13 mL TMEDA (99.6 mg, 0.860 mol, 4.00 eq.) added. After stirring the reaction mixture at room temperature overnight, an orange suspension was obtained which was diluted with 60 mL diethyl ether. 60.0 mg of **P1** (CMS: 80.7 µmol, 0.375 eq.) were dissolved in 20 mL diethyl ether and slowly added to the reaction mixture with the aid of a syringe pump (2 mL·h^{-1}). After complete addition, an orange solution containing a colorless precipitate was obtained. The precipitate was removed by filtration and the solvent removed from the filtrate under reduced pressure. The resulting orange solid was washed with *n*-hexane (5 x 5 mL). After drying, **1** was obtained as an off-white solid (50.0 mg).

^{1}H NMR (400 MHz, THF-d_8, 298 K): δ / ppm = 7.40-6.26 (br, aromatic), 2.37-1.02 (br, aliphatic backbone).

SEC (DMAc, RI, PS cal.): M_n = 11,900 g·mol^{-1}, M_p = 12,400 g·mol^{-1}, $Đ$= 1.18.

DLS (THF): D_h = 4.68 nm.

DOSY (400 MHz, THF-d_8, 298 K): D = 1.99·10^{-10} m^2·s^{-1}.

3.4 Synthesis of SCNP 2

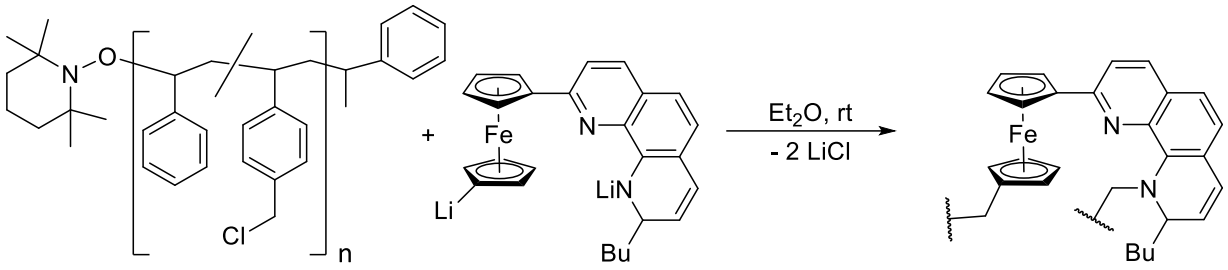

214 mg 2-Ferrocenyl-1,10-phenanthroline (0.588 mol, 1.00 eq.) were dissolved in 40 mL of diethyl ether and 0.94 mL *n*-BuLi (2.5 M in hexane, 2.35 mmol, 4.00 eq.) and 0.35 mL TMEDA (271 mg, 2.35 mmol, 4.00 eq.) were added. An immediate color change from orange to dark red occurred. The solution was stirred at room temperature overnight and subsequently diluted with 40 mL of diethyl ether. 167 mg **P1** (CMS: 0.224 mmol, 0.382 eq.) were dissolved in 20 mL of diethyl ether and slowly added to the reaction mixture with the aid of a syringe pump (3 mL·h^{-1}). After complete addition, a dark red suspension was obtained. The precipitate was removed by filtration and the solvent removed from the filtrate under reduced pressure. The resulting dark red solid was washed with methanol until the washings were nearly colorless (about 200 mL). After drying, **2** was obtained as an orange solid (80.0 mg).[a,b]

^{1}H NMR (400 MHz, THF-d_8, 298 K): δ / ppm = 7.40-6.20 (br, aromatic), 2.42-0.54 (br, aliphatic backbone).[c]

SEC (DMAc, RI, PS cal.): M_n = 14,700 g·mol^{-1}, M_p = 14,200 g·mol^{-1}, $Đ$= 1.27.[c]

DLS (THF): D_h = 5.35 nm.[c]

DOSY (400 MHz, THF-d_8, 298 K): D = 1.13·10^{-10} m^2·s^{-1}.[c]

UV/Vis (DCM): λ_{max} = 384 nm.

[a] The exact chemical structure of the crosslinking unit of **2** is unknown. Therefore, depicted structures are simplified and should only be regarded as illustrative (see Chapter 5.2 for details).

[b] The product contains an unidentified low molar mass impurity included in the given mass.

[c] The low molar mass impurity is not considered.

3.5 Synthesis of SCNP 2-Pd

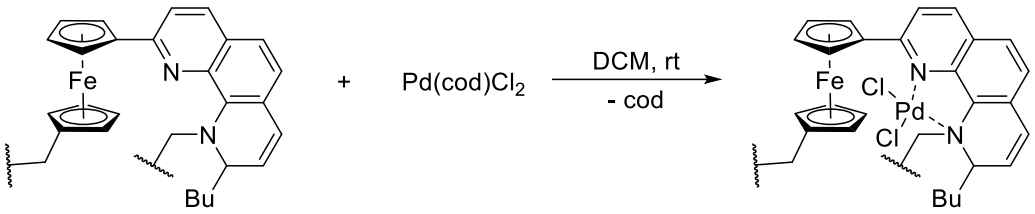

2 **2-Pd**

30.0 mg SCNP **2** (Phen: 20.2 µmol, 1.00 eq.)[d,e] were dissolved in 10 mL of DCM. 10.0 mg [Pd(cod)Cl_2] (35.0 µmol, 1.74 eq.) were dissolved in DCM and added to the solution of **2**. The resulting orange solution was stirred at room temperature overnight to give a dark red solution. The solvent was removed under reduced pressure and the obtained dark red solid redissolved in a minimum quantity DCM. Precipitation in cold methanol gave a black solid which was collected by filtration and washed with methanol (3 x 5 mL). The solid was dried under reduced pressure to give **2-Pd** as black solid (20.0 mg).[d]

^{1}H NMR (400 MHz, THF-d_8, 298 K): δ / ppm = 7.82-6.06 (br, aromatic), 4.54-4.15 (br), 2.62-0.44 (br, aliphatic backbone).

SEC (DMAc, RI, PS cal.): M_n = 17,700 g·mol^{-1}, M_p = 16,600 g·mol^{-1}, $Đ$= 1.29.

DOSY (400 MHz, THF-d_8, 298 K): $D = 1.35 \cdot 10^{-10}$ m^2·s^{-1}.

EDX: Energy / keV = 0.28 (C-K$_\alpha$), 0.7 (Fe-L$_\alpha$), 2.6 (Cl-K$_\alpha$), 2.8 (Pd-L$_\alpha$), 6.4 (Fe-K$_\alpha$).

UV/Vis (DCM): λ_{max} = 401 nm, 568 nm.

[d] The exact chemical structure of the crosslinking unit of **2** is unknown. Therefore, depicted structures of **2** and **2-Pd** are simplified and should only be regarded as illustrative (see Chapter 5.2 for details).

[e] SCNP **2** contains an unidentified low molar mass impurity included in the given mass.

3.6 Catalytic Application of SCNP 2-Pd

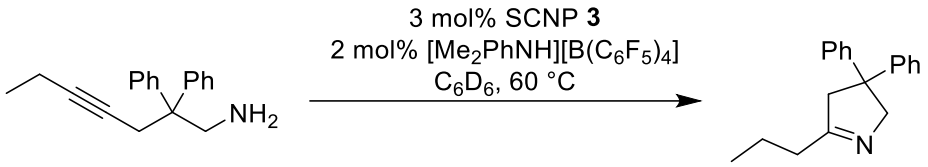

5.0 mg of Pd-SCNP **2-Pd** (Pd: 3.36 µmol, 0.0295 eq.) and 2.0 mg dimethylanilinium tetrakis-(pentafluorophenyl)borate (2.50 µmol, 0.0219 eq.) were dissolved in 0.5 mL of C_6D_6 in a NMR tube equipped with a J. Young valve. 30.0 mg 2,2-Diphenyl-4-heptyn-1-amine (0.114 mmol, 1.00 eq.) were added and the tube immediately inserted into a Bruker Avance Neo 400 MHz spectrometer. The reaction mixture was heated to 333 K inside the spectrometer using a Bruker Smart VT unit and ^{1}H NMR spectra recorded over a period of three hours.

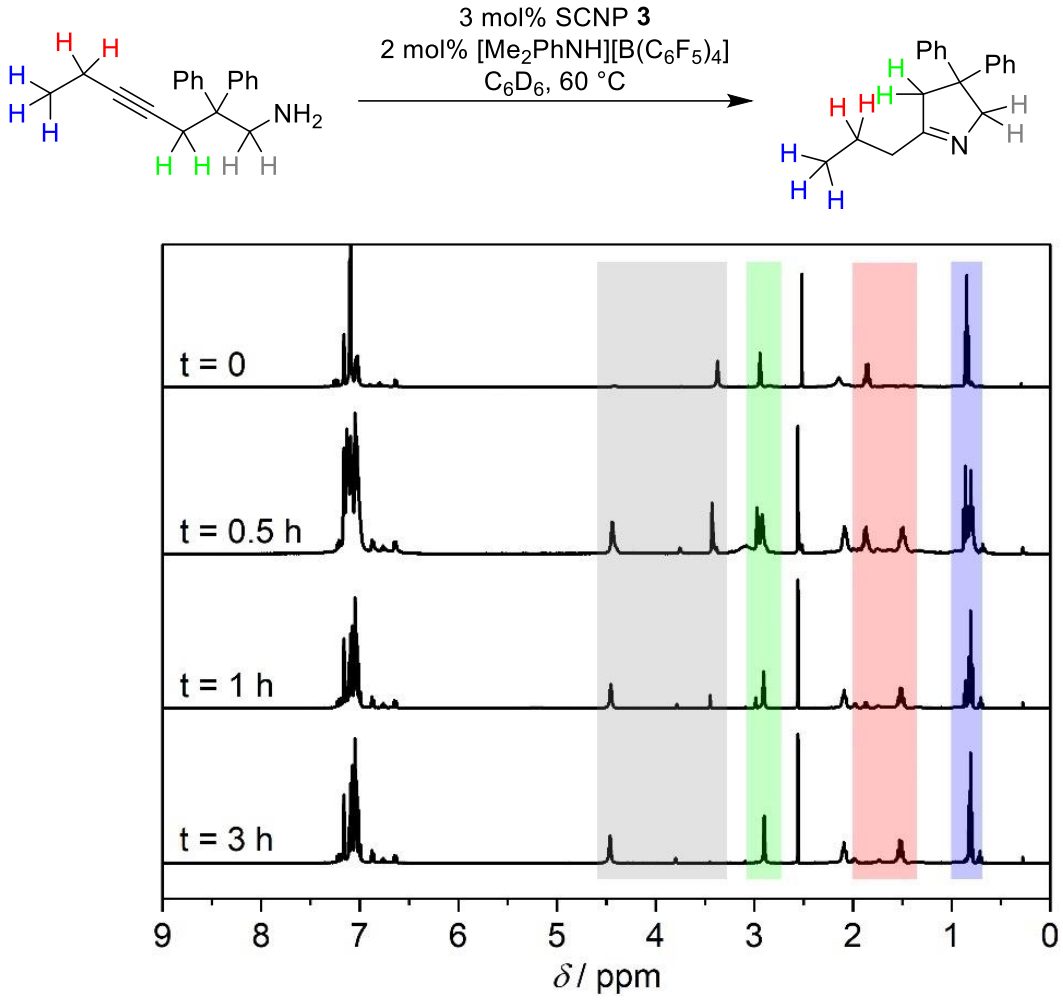

Figure S1 Reaction equation and stacked ^{1}H NMR spectra (400 MHz, C_6D_6, 333 K) illustrating the progress of the catalytic intramolecular hydroamination of 2,2-diphenyl-4-heptyn-1-amine.

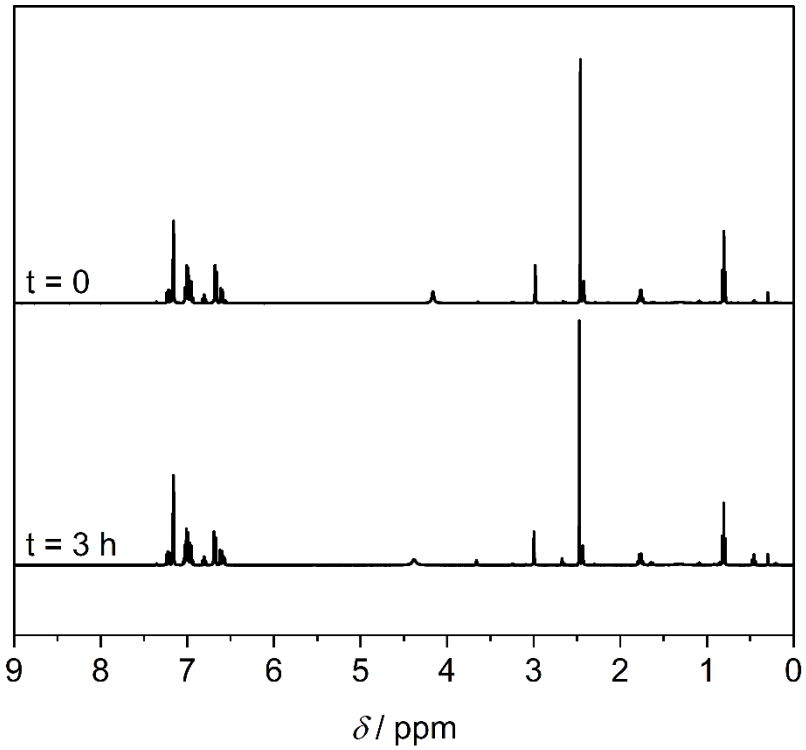

Figure S2 ^{1}H NMR spectra (400 MHz, C_6D_6, 298 K) of 2,2-diphenyl-4-heptyn-1-amine directly after addition of dimethylanilinium tetrakis(pentafluorophenyl)borate (t = 0) and after heating the mixture to 60 °C for three hours (t = 3 h).

4 Analytical Data

4.1 Nuclear Magnetic Resonance (NMR) Spectra

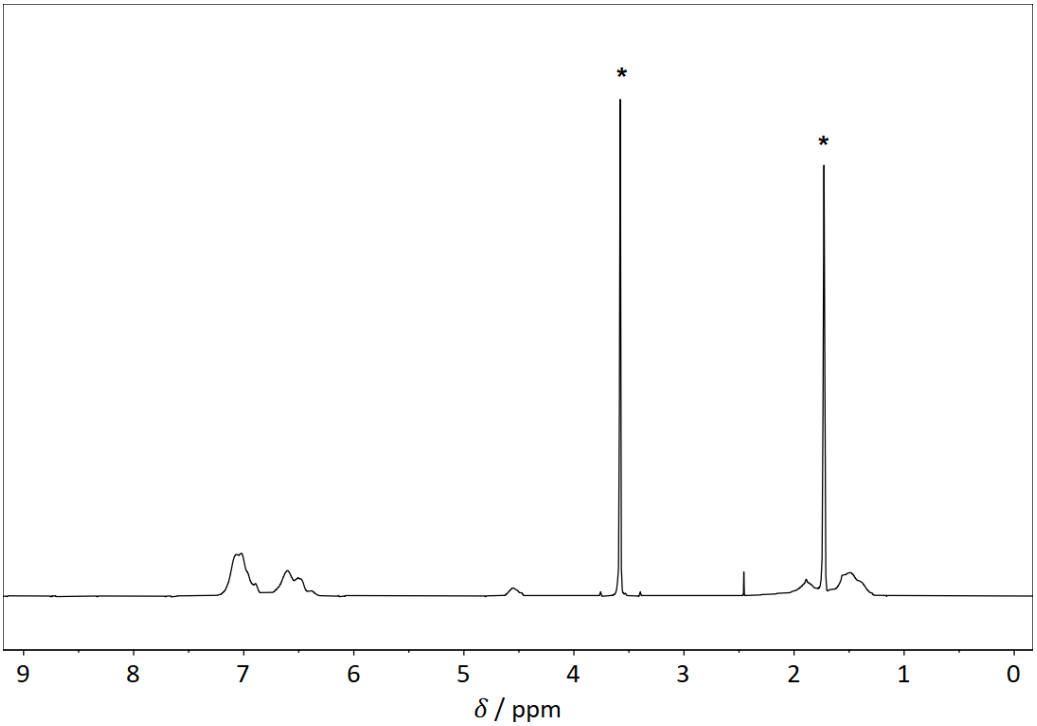

Figure S3 ^{1}H NMR spectrum (400 MHz, THF-d_8, 298 K) of polymer **P1**. * Residual solvent resonance.

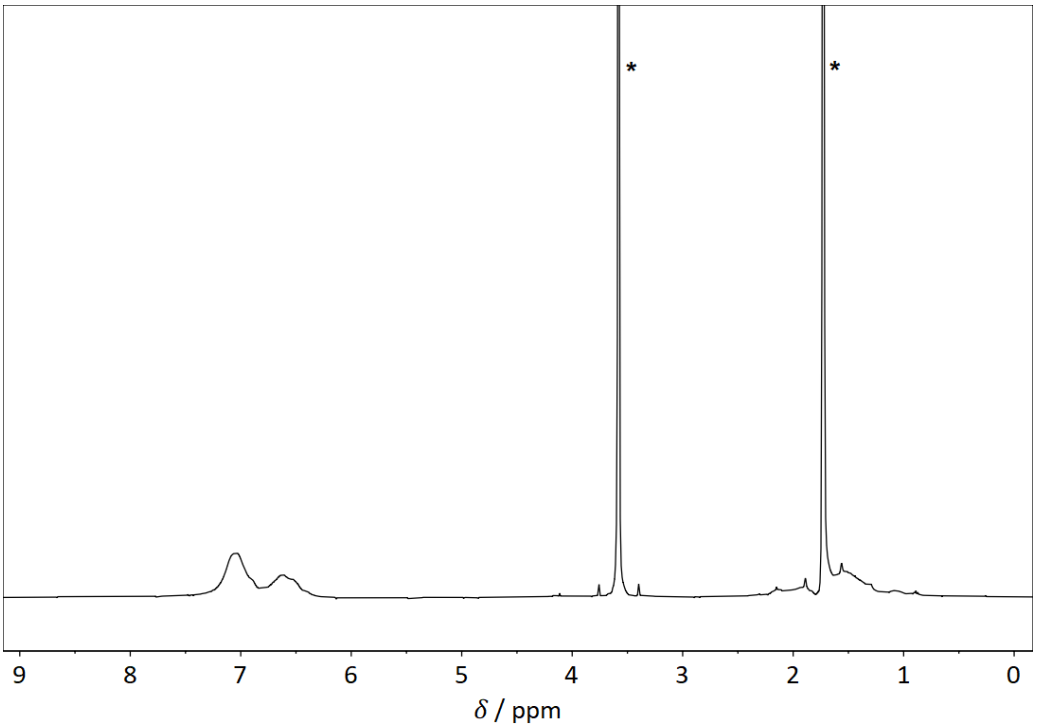

Figure S4 ^{1}H NMR spectrum (400 MHz, THF-d_8, 298 K) of SCNP **1**. * Residual solvent resonance.

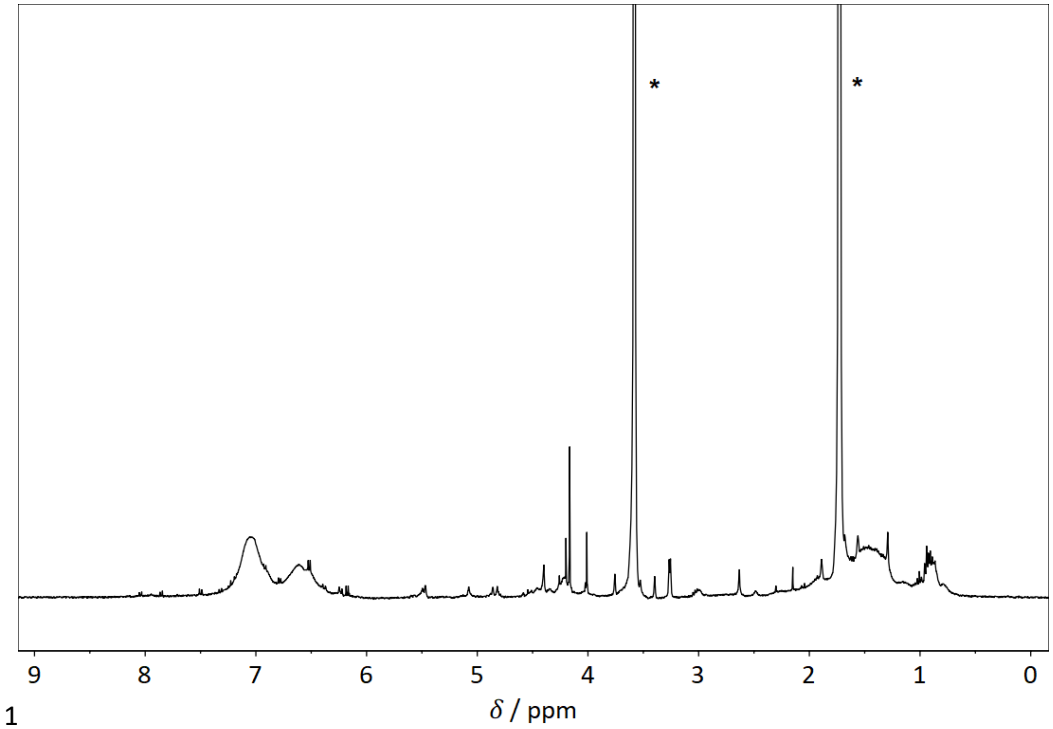

Figure S5 ^{1}H NMR spectrum (400 MHz, THF-d_8, 298 K) of SCNP **2**. * Residual solvent resonance. The presence of a small molecule impurity is evident from the spectrum.

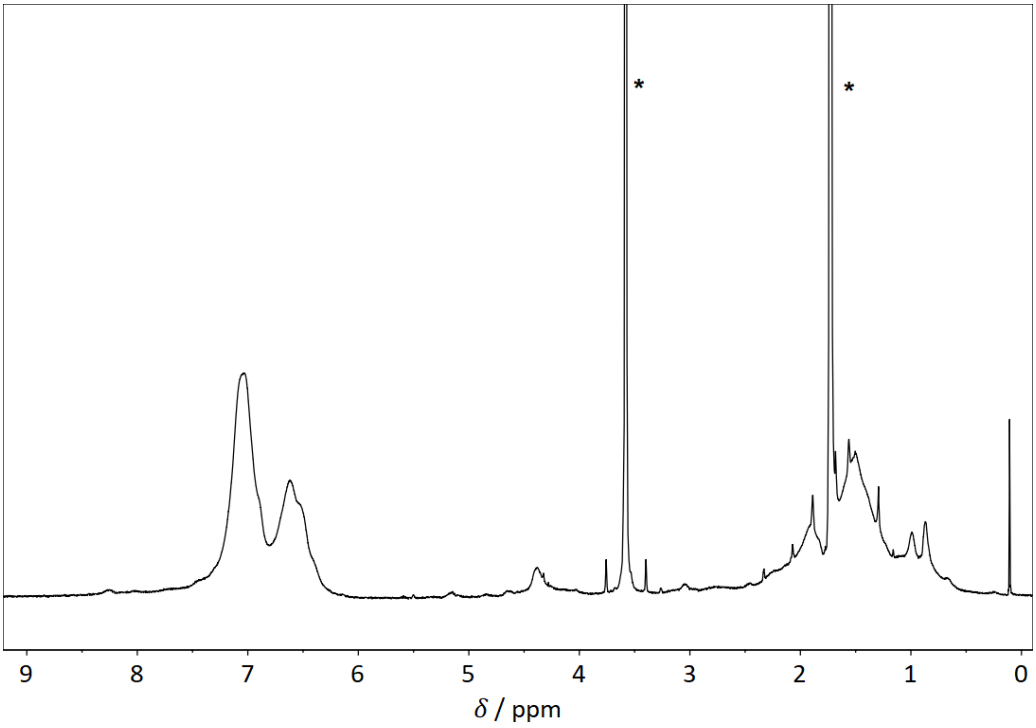

Figure S6 ^{1}H NMR spectrum (400 MHz, THF-d_8, 298 K) of SCNP **2-Pd**. * Residual solvent resonance.

4.2 Size Exclusion Chromatography (SEC) Data

Table S1 Number averaged (M_n) and peak (M_p) molar masses as well as dispersity index ($Đ$) of **P1**, **1**, **2** and **2-Pd**.

	M_n / g·mol^{-1}	M_p / g·mol^{-1}	$Đ$
Polymer **P1**	16,300	17,900	1.15
SCNP **1**	11,900	12,400	1.18
SCNP **2**	14,700	14,200	1.27
SCNP **2-Pd**	17,700	16,600	1.29

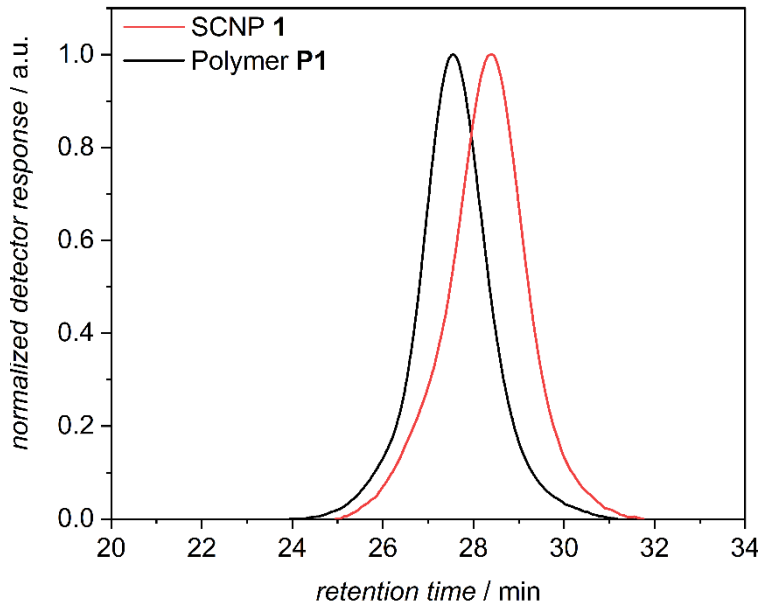

Figure S7 SEC chromatograms (DMAc, RI) of polymer **P1** (black) and SCNP **1** (red).

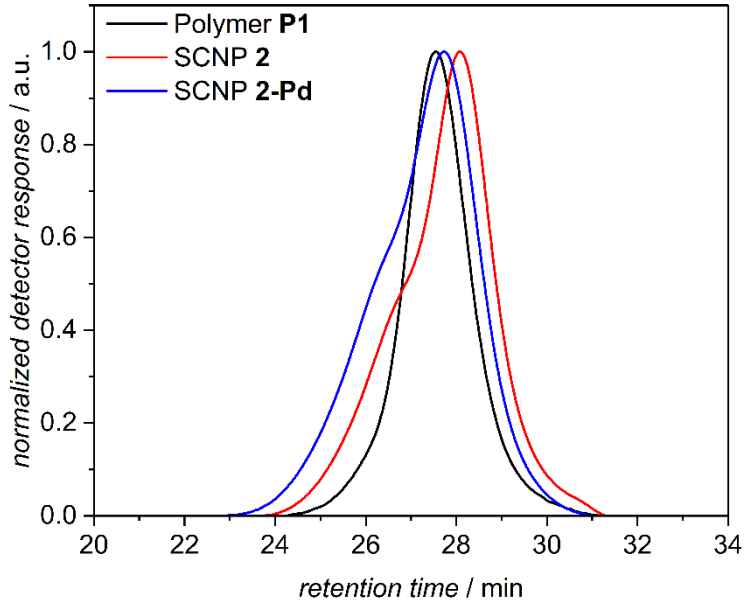

Figure S8 SEC chromatograms (DMAc, RI) of polymer **P1** (black), SCNP **2** (red) and SCNP **2-Pd** (blue).

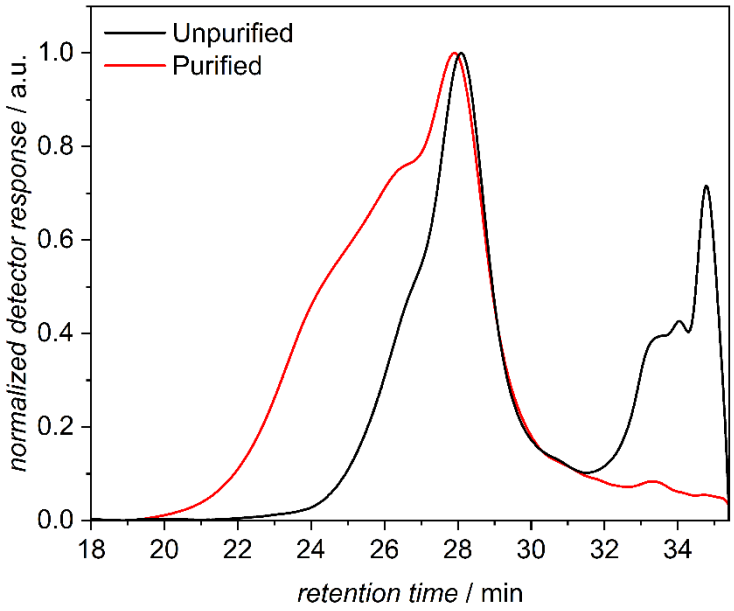

Figure S9 Superimposed SEC chromatograms (DMAc, RI) of unpurified SCNP **2** (black) and crosslinked polymer obtained after purification of **2** by preparative SEC (red). Note that the red curve is only representative of the soluble fraction of the sample obtained after purification.

4.3 Dynamic Light Scattering (DLS) Data

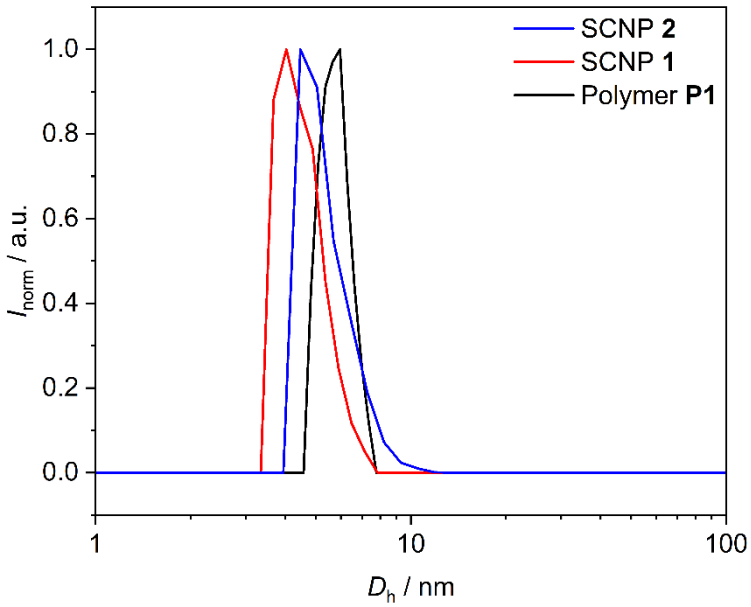

Figure S10 Number averaged size distributions of **P1** (black), SCNP **1** (red) and SCNP **2** (blue) obtained by DLS measurements in THF at 298 K.

4.4 Diffusion-Ordered Nuclear Magnetic Resonance (DOSY) Spectra

Polymer P1:

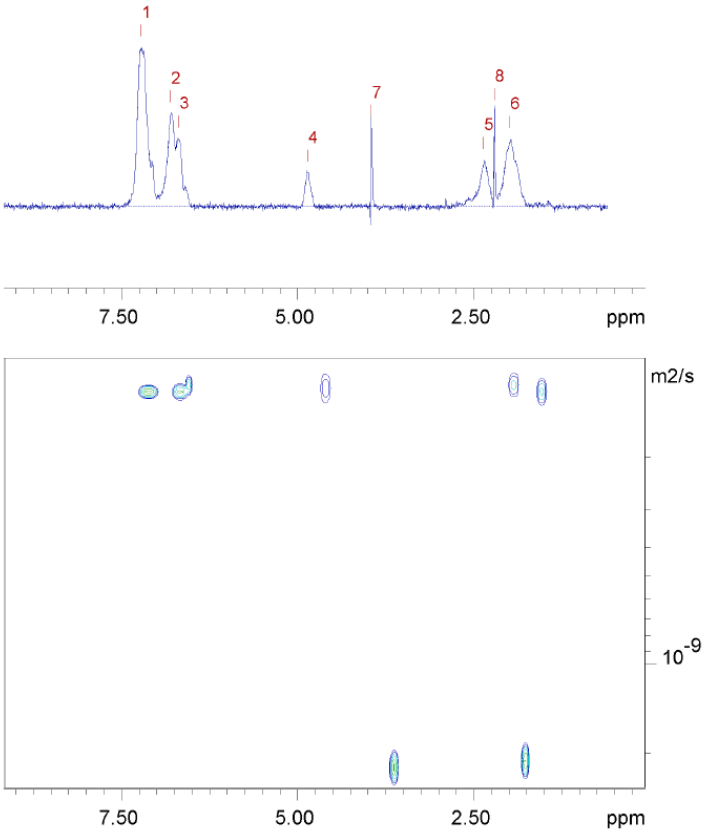

Figure S11 DOSY NMR spectrum (400 MHz, THF-d_8, 298 K) of polymer **P1**.

Table S2 Details of parameters and calculated values of DOSY measurements of polymer **P1**.

Fitted function:	f (x) = Io * exp (-D * x^2 * gamma^2 * littleDelta^2 (bigDelta-littleDelta/3)* 10^4
used gamma:	26752 rad/(s*Gauss)
used little delta:	0.0056000 s
used big delta:	0.099900 s
used gradient strength:	variable
Random error estimation of data:	RMS per spectrum (or trace/plane)
Systematic error estimation of data:	worst case per peak scenario
Fit parameter Error estimation method:	from fit using arbitray y uncertainties
Confidence level:	95%
Used peaks:	
Used integrals:	peak intensities
Used Gradient strength:	all values (including replicates) used

Peak name	F2 [ppm]	offset	offsetError	Io	error	D [m2/s]	error	fitInfo
1	7.103	3.79e+07	3.207e+06	3.57e+08	4.487e+06	1.19e-10	4.217e-12	Done
2	6.657	1.42e+07	2.625e+06	2.17e+08	3.669e+06	1.19e-10	5.655e-12	Done
3	6.534	1.08e+07	2.614e+06	1.60e+08	3.537e+06	1.14e-10	7.129e-12	Done
4	4.591	6.15e+06	2.622e+06	7.69e+07	3.628e+06	1.17e-10	1.561e-11	Done
5	1.932	6.07e+06	2.538e+06	1.02e+08	3.447e+06	1.14e-10	1.094e-11	Done
6	1.536	9.14e+06	3.499e+06	1.53e+08	4.890e+06	1.19e-10	1.068e-11	Done
7	3.625	1.35e+07	2.730e+06	3.20e+08	1.344e+07	2.24e-09	2.135e-10	Done
8	1.771	1.07e+07	2.627e+06	3.01e+08	1.272e+07	2.13e-09	2.049e-10	Done

SCNP 1:

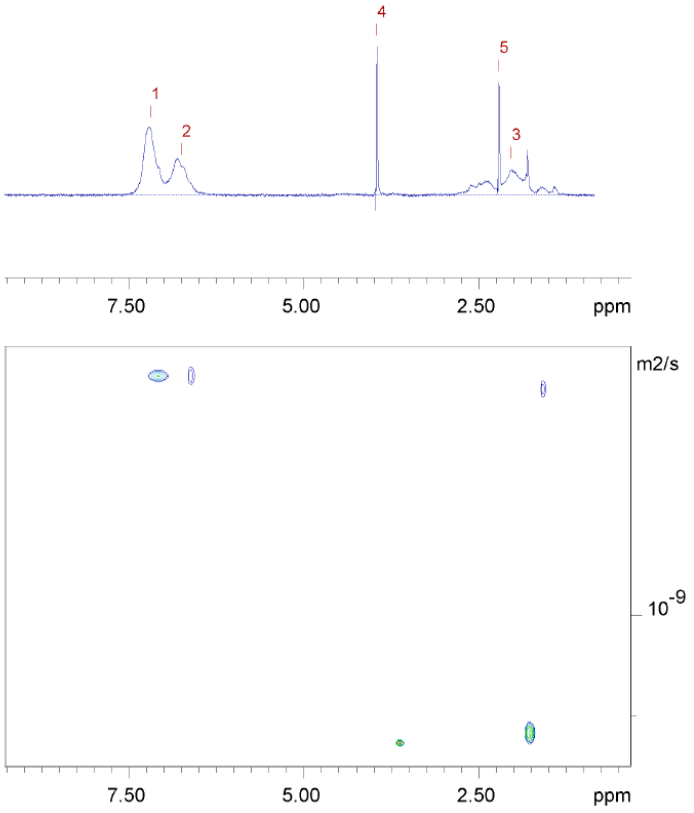

Figure S12 DOSY NMR spectrum (400 MHz, THF-d_8, 298 K) of SCNP **1**.

Table S3 Details of parameters and calculated values of DOSY measurements of SCNP **1**.

Fitted function:	f (x) = Io * exp (-D * x^2 * gamma^2 * littleDelta^2 (bigDelta-littleDelta/3)* 10^4
used gamma:	26752 rad/(s*Gauss)
used little delta:	0.0048000 s
used big delta:	0.099900 s
used gradient strength:	variable
Random error estimation of data:	RMS per spectrum (or trace/plane)
Systematic error estimation of data:	worst case per peak scenario
Fit parameter Error estimation method:	from fit using arbitray y uncertainties
Confidence level:	95%
Used peaks:	
Used integrals:	peak intensities
Used Gradient strength:	all values (including replicates) used

Peak name	F2 [ppm]	offset	offsetError	Io	error	D [m2/s]	error	fitInfo
1	7.066	3.94e+06	3.147e+05	4.99e+07	4.956e+05	1.93e-10	5.217e-12	Done
2	6.596	1.56e+06	3.582e+05	2.22e+07	5.677e+05	1.95e-10	1.353e-11	Done
3	1.585	1.07e+06	3.027e+05	1.90e+07	5.033e+05	2.10e-10	1.494e-11	Done
4	3.626	1.54e+06	3.356e+05	3.42e+08	1.527e+06	2.40e-09	2.458e-11	Done
5	1.774	8.74e+06	9.056e+05	2.21e+08	4.019e+06	2.23e-09	9.288e-11	Done

SCNP 2:

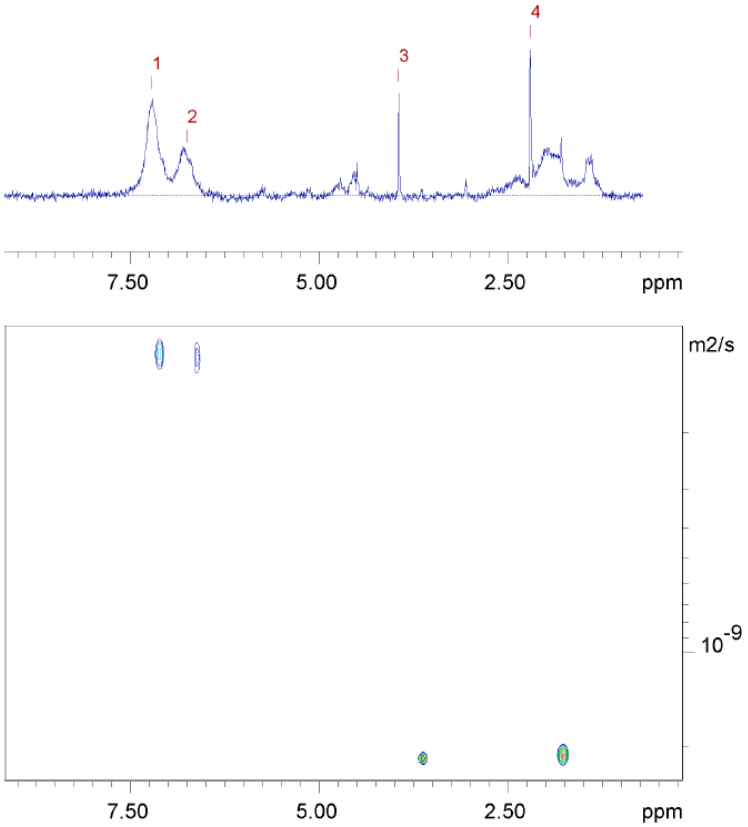

Figure S13 DOSY NMR spectrum (400 MHz, THF-d_8, 298 K) of SCNP **2**.

Table S4 Details of parameters and calculated values of DOSY measurements of SCNP **2**.

Fitted function:	f (x) = Io * exp (-D * x^2 * gamma^2 * littleDelta^2 (bigDelta-littleDelta/3)* 10^4
used gamma:	26752 rad/(s*Gauss)
used little delta:	0.0048000 s
used big delta:	0.099900 s
used gradient strength:	variable
Random error estimation of data:	RMS per spectrum (or trace/plane)
Systematic error estimation of data:	worst case per peak scenario
Fit parameter Error estimation method:	from fit using arbitray y uncertainties
Confidence level:	95%
Used peaks:	
Used integrals:	peak intensities
Used Gradient strength:	all values (including replicates) used

Peak name	F2 [ppm]	offset	offsetError	Io	error	D [m2/s]	error	fitInfo
1	7.103	3.23e+06	7.710e+05	2.58e+07	8.368e+05	1.12e-10	1.069e-11	Done
2	6.608	9.07e+05	5.075e+05	1.15e+07	5.569e+05	1.14e-10	1.624e-11	Done
3	3.626	9.99e+05	5.387e+05	3.14e+08	2.374e+06	2.18e-09	3.792e-11	Done
4	1.774	1.29e+07	1.105e+06	2.90e+08	4.811e+06	2.10e-09	8.047e-11	Done

SCNP 2-Pd:

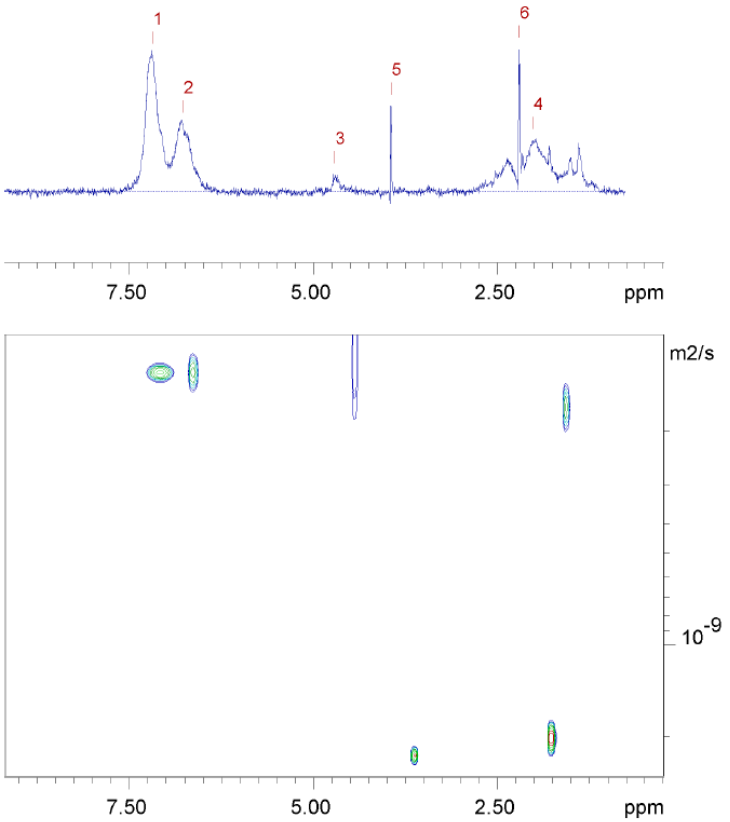

Figure S14 DOSY NMR spectrum (400 MHz, THF-d_8, 298 K) of SCNP **2-Pd**.

Table S5 Details of parameters and calculated values of DOSY measurements of SCNP **2-Pd**.

Fitted function:	f (x) = Io * exp (-D * x^2 * gamma^2 * littleDelta^2 (bigDelta-littleDelta/3)* 10^4
used gamma:	26752 rad/(s*Gauss)
used little delta:	0.0048000 s
used big delta:	0.099900 s
used gradient strength:	variable
Random error estimation of data:	RMS per spectrum (or trace/plane)
Systematic error estimation of data:	worst case per peak scenario
Fit parameter Error estimation method:	from fit using arbitray y uncertainties
Confidence level:	95%
Used peaks:	
Used integrals:	peak intensities
Used Gradient strength:	all values (including replicates) used

Peak name	F2 [ppm]	offset	offsetError	Io	error	D [m2/s]	error	fitInfo
1	7.066	1.56e+07	1.634e+06	1.52e+08	1.955e+06	1.29e-10	4.865e-12	Done
2	6.622	7.50e+06	2.002e+06	7.18e+07	2.374e+06	1.28e-10	1.234e-11	Done
3	4.432	1.64e+06	2.204e+06	1.44e+07	2.489e+06	1.19e-10	6.044e-11	Done
4	1.573	4.20e+06	1.874e+06	5.78e+07	2.659e+06	1.65e-10	2.128e-11	Done
5	3.621	7.76e+05	1.019e+06	2.94e+08	4.585e+06	2.32e-09	8.283e-11	Done
6	1.771	1.54e+07	2.667e+06	3.99e+08	1.145e+07	2.02e-09	1.333e-10	Done

4.5 Energy Dispersive X-Ray Spectroscopy (EDX) Data

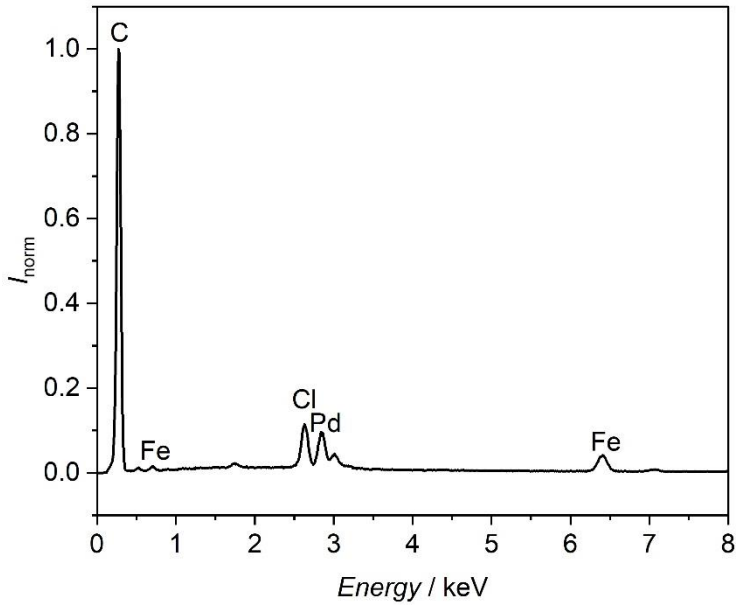

Figure S15 EDX spectrum of **2-Pd**. Peaks are labelled with the symbols of the elements they are characteristic for.

Table S6 Composition of **2-Pd** determined by EDX. Note that the sample was prepared on a conductive carbon pad. Values given for C are therefore not interpretable. Also note that the absolute amount of the other elements compared to C is too low to allow for quantitative analysis of the composition.

Element/Emission	Wt%	At%
C/K_α	92.18	97.70
O/K_α	1.35	1.09
Cl/K_α	1.54	0.45
Pd/L_α	3.25	0.39
Fe/L_α	1.67	0.37

4.6 UV/Vis Spectra

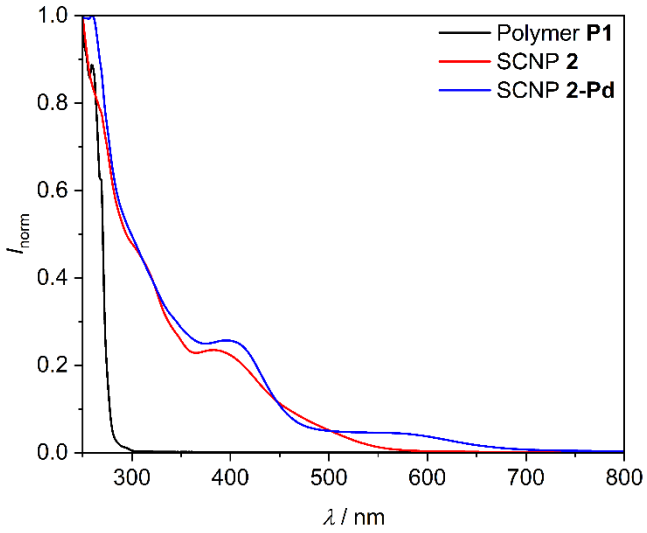

Figure S16 Superimposed UV/Vis spectra (DCM, 298 K) of polymer **P1** (black), SCNP **2** (red) and SCNP **2-Pd** (blue).

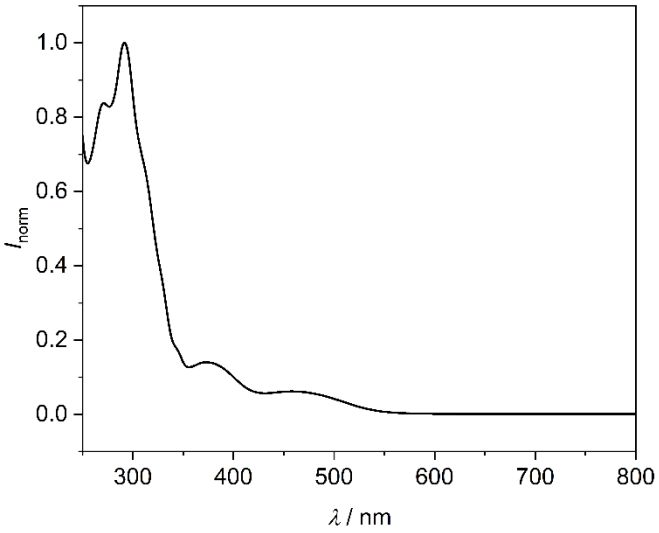

Figure S17 UV/Vis spectrum (DCM, 298 K) of 2-ferrocenyl-1,10-phenanthroline.

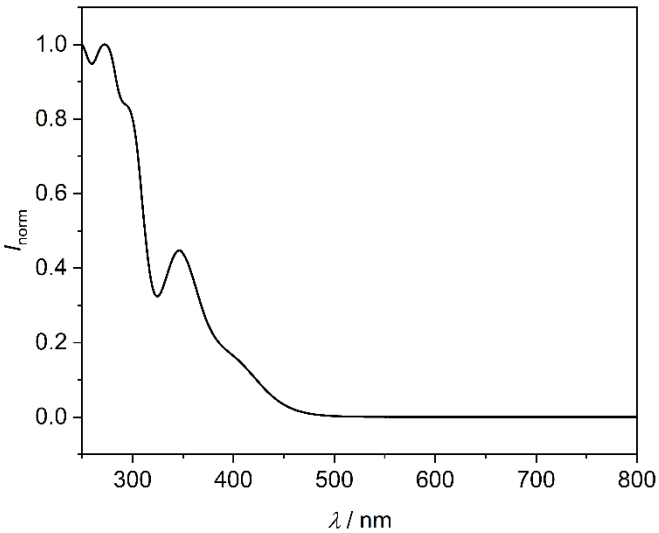

Figure S18 UV/Vis spectrum (DCM, 298 K) of dichloro-(1,5-cyclooctadiene)-palladium(II).

5 Quantum Chemical Calculations

5.1 Computational Details

Quantum chemical calculations at density functional theory (DFT) level were performed with the program suite TURBOMOLE.[4,5] For all calculations, the PBE0 hybrid functional[6,7] was employed. dhf-TZVP basis sets[8-10] together with the effective core potential (ECP) for Pd (ECP-28)[11] were used. The resolution of the identity approximation for the Coulomb part (RI-*J*) in combination with the corresponding auxiliary basis sets was employed in all cases.[12,13] Self-consistent field (SCF) thresholds were set to 10^{-7} E_h. For response calculations, the convergence criterion for the root mean square of the density matrix was set to 10^{-7} E_h. Medium sized multigrids (gridsize m3)[14,15] were used for the numerical integration of the exchange-correlation terms. In all calculations, the D4 dispersion correction was employed.[16] Difference densities were analyzed using the python script PANAMA (**P**eak **ANA**lyzing **MA**chine).[17] Cartesian coordinates of all optimized structures are given within the separate file *optimized-structures.pdf*.

Nucleophilic attack of *n*-BuLi on 2-ferrocenyl-1,10-phenanthroline gives rise to stereocenters on the 1,10-phenanthroline moiety. As no chiral auxiliary is added, racemic mixtures are obtained. Only one of the existing stereoisomers is considered in the calculations reported here. For all molecules different conformations exist for which rapid interconversion is expected to take place in solution at room temperature. Only the energetically most favorable conformation in each case is reported here. The latter was determined by performing geometry optimizations starting from a number of different chemically reasonable conformations.
The TMEDA present in the reaction mixture throughout the synthesis of SCNP **2** is not considered in the calculations. While additional coordination of TMEDA to the Li ions is expected to contribute to the overall stability of the structures, this should not lead to a qualitative change of the overall picture discussed here.

5.2 Experimental and Quantum Chemical Study of the Folding Unit of SCNP 2

To obtain SCNP **2**, 2-ferrocenyl-1,10-phenanthroline is lithiated *in situ* by addition of an excess of *n*-BuLi and subsequently reacted with polymer **P1** (see 3.4 for details).
When only the cyclopentadienyl (Cp) rings of 2-ferrocenyl-1,10-phenanthroline are taken into consideration, lithiation can already occur in three chemically distinct positions when a free rotation of the Cp rings around the pseudo-C_5 axis and of the phenanthroline moiety around its bond to the ferrocene unit is assumed. Furthermore, it is known from the literature, that 1,10-phenanthroline itself undergoes nucleophilic attack by *n*-BuLi in the 2-position, leading to accumulation of electron density on the neighboring nitrogen atom which in turn makes it nucleophilic.[18-20] A reaction of 1,10-phenanthroline, *n*-BuLi and benzyl bromide leading to 2-butyl-1,2-dihydro-1-(phenylmethyl)-1,10-phenanthroline is reported in the literature.[20] Similarly, reaction of 6-ferrocenyl-2,2'-bipyridine with *n*-BuLi leads to 6-ferrocenyl-6'-*n*-butyl-2,2'-bipyridine as well as an unidentified dibutylated derivative of 6-ferrocenyl-2,2'-bipyridine.[21]

It thus is plausible, that analogous reactions occur in the case reported here when 2-ferrocenyl-1,10-phenanthroline is reacted with *n*-BuLi. Based on the literature outlined above, it is expected that in a first step the lithium salt of 2-ferrocenyl-9,10-dihydro-9-*n*-butyl-1,10-phenanthroline is formed. Without further lithiation, the lithiated nitrogen atom of this species can act as a nucleophile and react with the chloromethyl styrene moieties in **P1** upon its addition. However, this does not lead to single-chain nanoparticle folding and is one potential reason for the small shoulder towards short retention times in the SEC chromatogram of **2**. To achieve single-chain folding, a second lithiation is necessary, which can either take place on the Cp rings of the ferrocene moiety or result from a second butylation step.

To get a more detailed understanding of the lithiation process beyond the outlined literature, combined experimental and quantum chemical studies were undertaken.

Experimentally, 2-ferrocenyl-1,10-phenanthroline was reacted with *n*-BuLi and TMEDA in diethyl ether, similar as described in Chapter 3.4. However, instead of adding **P1**, the reaction mixture was quenched with D_2O. The ^1H NMR spectrum of the product obtained after evaporation of the solvent as well as that of 2-ferrocenyl-1,10-phenanthroline is shown in Figure S19. The reaction product features new resonances at δ = 1.88-0.60 ppm, going in line with the presence of butyl groups. Additionally, an upfield shift of the resonances of the former phenanthroline moiety is evident compared to the starting material, indicating a partial dearomatization of the phenanthroline rings. Resonances between δ = 4.34-3.82 ppm can be assigned to protons of the ferrocene unit. However, due to resonance overlap, a definite interpretation of the NMR spectrum is out of reach. Additional ^2H NMR measurements were also unsuccessful.

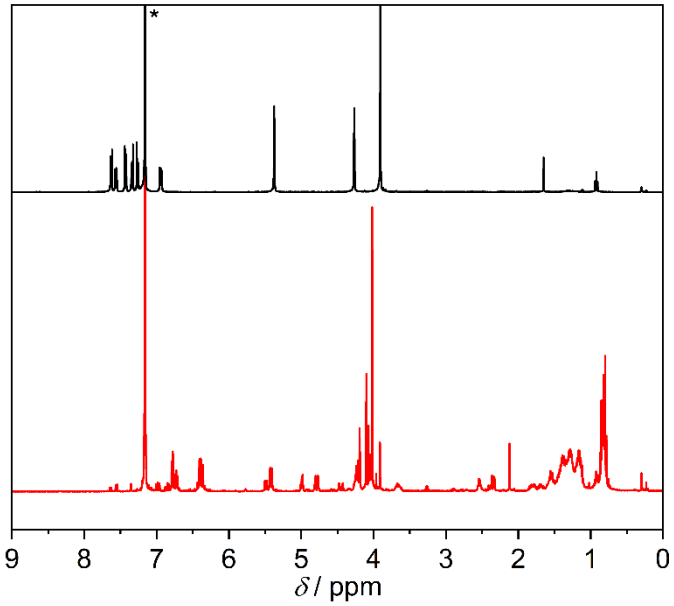

Figure S19 Stacked ^1H NMR spectra (400 MHz, C_6D_6, 298 K) of 2-ferrocenyl-1,10-phenanthroline (black) and the product mixture obtained after reaction of 2-ferrocenyl-1,10-phenanthroline with *n*-BuLi and subsequent quenching with D_2O (red). * Residual solvent resonance.

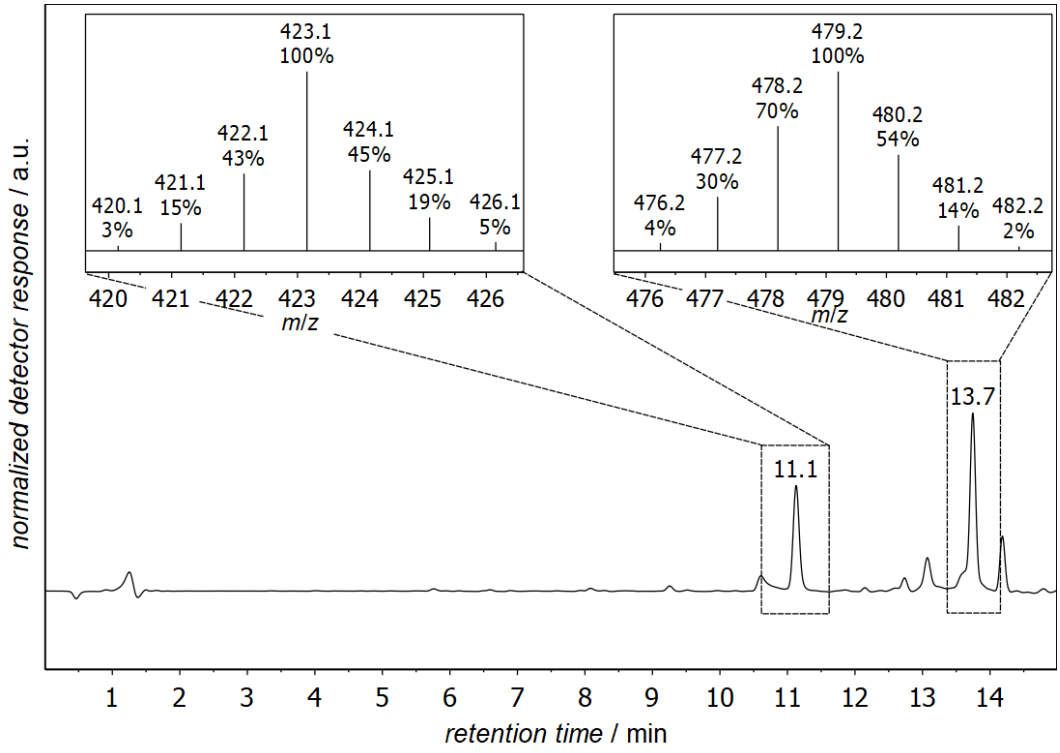

Figure S20 LC chromatogram (254 nm detector wavelength) of the mixture obtained after reaction of 2-ferrocenyl-1,10-phenanthroline with *n*-BuLi and subsequent quenching with D_2O. Inserts show the relevant region of the accumulated mass spectra (positive mode) of the corresponding peaks.

The LC chromatogram (see Figure S20) clearly shows that different products are formed throughout the reaction. The mass spectra corresponding to the most intense peaks (at 11.1 and 13.7 minutes retention time) are depicted in Figure S20 and corroborate the NMR results. With *m/z* values of 423.1 (11.1 minutes) and 479.2 (13.7 minutes), the formation of monobutylated and dibutylated derivatives of 2-ferrocenyl-1,10-phenanthroline is evident. The isotopic pattern is reminiscent of that of Fe (natural abundance: ^{54}Fe 6 %, ^{56}Fe 92 %, ^{57}Fe 2%, ^{58}Fe 0.3%). However, due to peak overlap of different species, the natural abundance ratio is not resembled.

To conclude, the reaction of 2-ferrocenyl-1,10-phenanthroline with *n*-BuLi yields a mixture of differently substituted derivatives of the starting material. The pronounced overlap of resonances in the NMR spectrum precludes an unambiguous determination of the location of the incorporated butyl groups as well as that of lithiation or deuteration, respectively.

To get further insights into the structure of the folding unit of SCNP **2**, beyond the experimentally accessible regime, quantum chemical calculations were performed. At first, the most probable positions for nucleophilic attack of the butyl groups were determined. The regioselectivity of the nucleophilic attack is influenced by steric considerations, the shape of the lowest unoccupied molecular orbital (LUMO) and the charge distribution within the attacked molecule. The LUMO of 2-ferrocenyl-1,10-phenanthroline is delocalized over the phenanthroline π-system (Figure S21 a). However, the only sterically accessible atom combining a large contribution to the LUMO with a positive natural population analysis[22] (NPA) charge is C-9 within the 1,10-phenanthroline moiety. Thus, nucleophilic attack by *n*-BuLi most likely occurs on this carbon atom, yielding the lithium salt of 2-ferrocenyl-9,10-dihydro-9-*n*-butyl-1,10-phenanth-

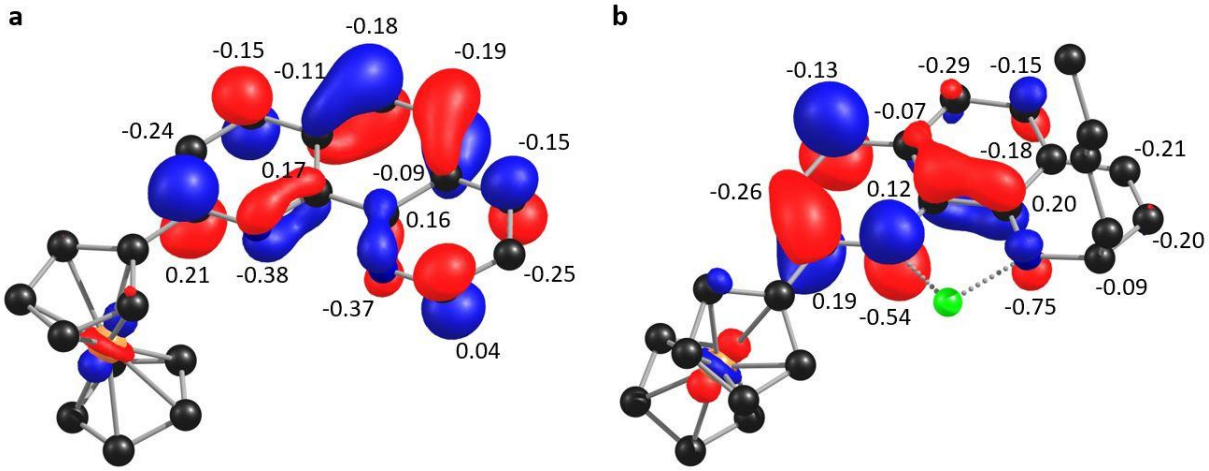

Figure S21 LUMO of 2-ferrocenyl-1,10-phenanthroline (a) and the lithium salt of 2-ferrocenyl-9,10-dihydro-9-*n*-butyl-1,10-phenanthroline (b) (PBE0/dhf-TZVP). Contours are drawn at 0.05 atomic units. Numbers denote NPA charges of the atoms of the phenanthroline moiety. Hydrogen atoms are omitted for clarity. Lithium green, carbon black, nitrogen blue, iron orange.

roline, which is in line with the literature discussed above. Based on the same line of reasoning, a second butyl group most probably attacks on C-4 of the 1,10-phenanthroline moiety of the latter species. Contributions of this carbon atom dominate the LUMO, and out of the sterically accessible carbon atoms, it is the one with the least negative NPA charge (Figure S21 b). Therefore, onefold and twofold butylation of 2-ferrocenyl-1,10-phenanthroline is expected to lead to the lithium salts of 2-ferrocenyl-9,10-dihydro-9-*n*-butyl-1,10-phenanthroline (Figure S22 a) and 2-ferrocenyl-1,4,9,10-tetrahydro-4,9-di(*n*-butyl)-1,10-phenanthroline (Figure S22 b), respectively. Reaction of the latter with the chloromethyl styrene moieties of **P1** would in principle allow for SCNP folding. However, additional quantum chemical calculations indicate that nucleophilic attack of both nitrogen atoms on the polymer requires a significant distortion of the phenanthroline moiety. Furthermore, it seems highly unlikely that the steric congestion in the resulting molecule would allow for subsequent metal complexation. Instead, it seems more likely that only one of the nitrogen atoms of the dibutylated derivative of 2-ferrocenyl-1,10-phenanthroline reacts with the polymer and the second lithiated site is quenched during the workup procedure. This might contribute to the shoulder towards short retention times in the SEC chromatogram of **2**.

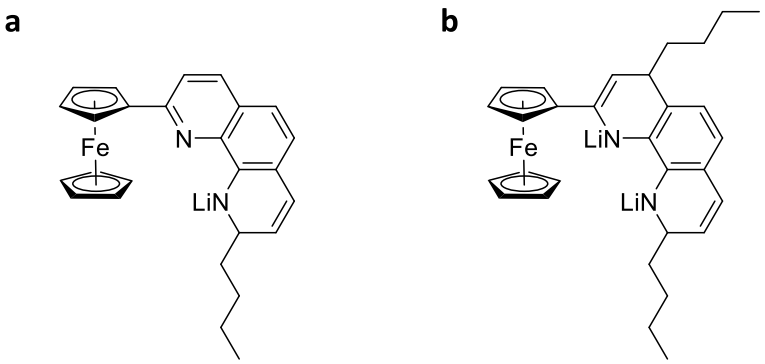

Figure S22 Chemical structure of 2-ferrocenyl-9,10-dihydro-9-*n*-butyl-1,10-phenanthroline (a) and 2-ferrocenyl-1,4,9,10-tetrahydro-4,9-di(*n*-butyl)-1,10-phenanthroline (b).

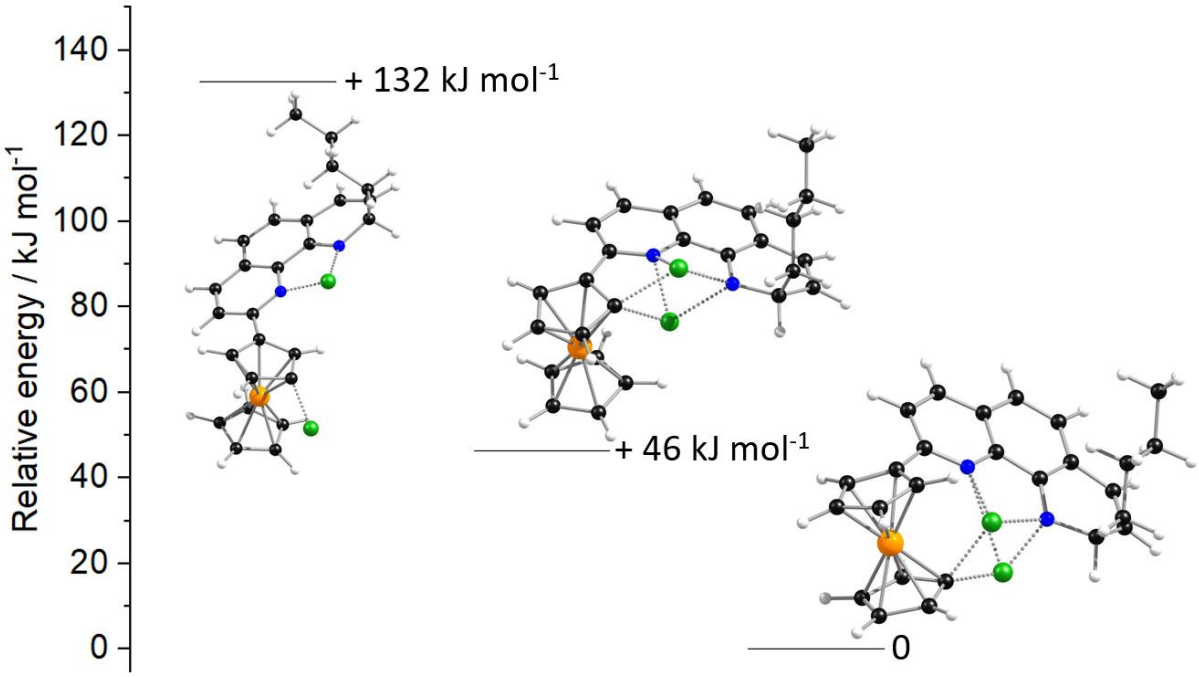

Figure S23 Relative energies (PBE0/dhf-TZVP) of the three chemically distinct dilithiated constitutional isomers of 2-ferrocenyl-9,10-dihydro-9-*n*-butyl-1,10-phenanthroline. Hydrogen white, lithium green, carbon black, nitrogen blue, iron orange.

To achieve SCNP folding with the monobutylated derivative of 2-ferrocenyl-1,10-phenanthroline, a second lithiation on one of the Cp rings is necessary. To shed light on where this most likely occurs, the energies of the three possible, chemically distinct, dilithiated constitutional isomers were compared (Figure S23). Taking the long reaction time for the lithiation step into account (refer to 3.4 for details), it is reasonable to assume that the reaction mixture reaches a state of thermodynamic equilibrium with the most stable isomer being the dominant species in the reaction solution. Comparing the relative energies of the different isomers reveals that it is energetically favorable when the second lithiation occurs in close spacial proximity to the nitrogen atoms due to additional coordination of the latter to the lithium ions. Additionally, it is evident that lithiation on the unsubstituted Cp ring is favored over lithiation on the substituted one (by about 50 kJ·mol^{-1}).

The NPA charges of the lowest energy isomer reveal that the negative charge is mainly centered on N-10 (-0.83) and the lithiated carbon of the unsubstituted Cp ring (-0.67). Inspection of the highest occupied molecular orbital (HOMO) shows no contributions of the lithiated carbon atom but large contributions of the lithiated nitrogen. Hence, nucleophilic substitution will preferably occur on N-10 when **P1** is added to the reaction mixture.

To investigate whether the additional aromatic group present after this initial nucleophilic substitution step could lead to a change in the position of the remaining lithiated site, model complexes with a 1-methyl-4-ethylbenzene substituent on N-10 were constructed and the relative energies of the two most stable constitutional isomers, with the lithium ion in close spacial proximity to the nitrogen atoms, were compared (Figure S24). Again, the isomer lithiated on the unsubstituted Cp ring proves to be energetically favored (by about 20 kJ·mol^{-1}). Note

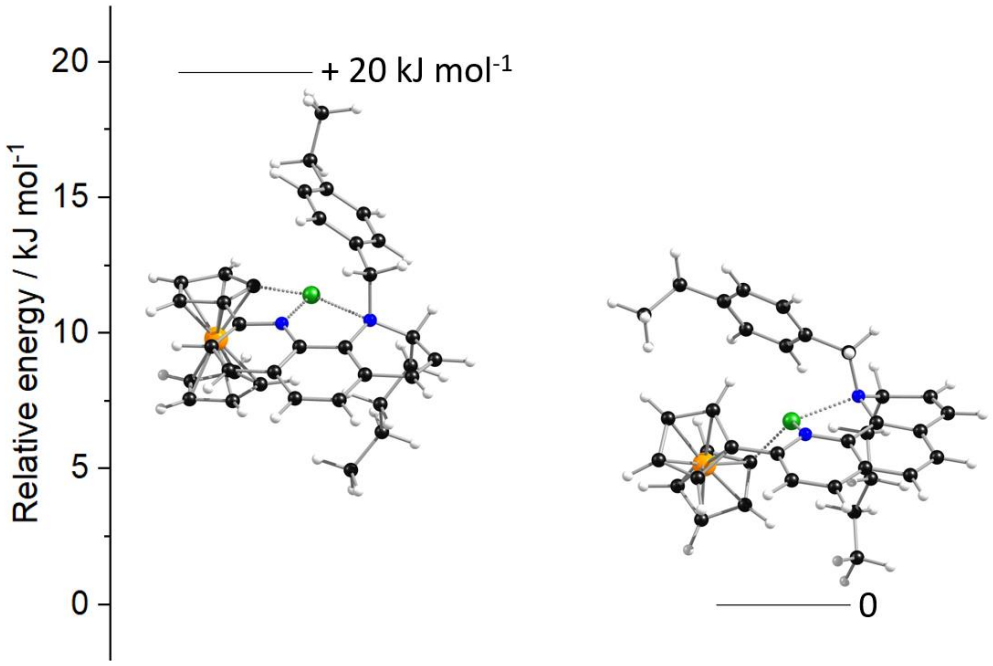

Figure S24 Relative energies (PBE0/dhf-TZVP) of the two lowest energy constitutional isomers of lithiated 2-ferrocenyl-9,10-dihydro-9-*n*-butyl-10-(4-ethylbenzyl)-1,10-phenanthroline. Hydrogen white, lithium green, carbon black, nitrogen blue, iron orange.

that the aromatic moiety contributes to the stabilization of the structures by coordination to the lithium ion. Reaction of the remaining lithiated site with the chloromethyl styrene moieties of **P1** leads to SCNP folding.

In summary, these results highlight the complexity of the mixture obtained after reaction of *n*-BuLi with 2-ferrocenyl-1,10-phenanthroline. Based on the experimental study, it is evident that monobutylated and dibutylated derivatives of 2-ferrocenyl-1,10-phenanthroline are the dominant species present in the reaction solution. The most probable location of the butyl groups was determined based on quantum chemical calculations. Sterical considerations render SCNP folding due to a reaction of both nitrogen atoms of the lithium salt of 2-ferrocenyl-1,4,9,10-tetrahydro-4,9-di(*n*-butyl)-1,10-phenanthroline with the polymer highly unlikely. It seems more plausible that a second lithiation occurs on the Cp rings of the ferrocene moiety after onefold butylation, and that SCNP folding in **2** is dominantly achieved by reaction of dilithiated 2-ferrocenyl-9,10-dihydro-9-*n*-butyl-1,10-phenanthroline on N-10 and one the five chemically equivalent carbon atoms of the unsubstituted Cp ring.

5.3 Study of Optical Absorption Properties of 2 and 2-Pd

The UV/Vis spectra (see Figure S16) as well as the perceivable colors of solutions of **P1** (colorless), **2** (yellow) and **2-Pd** (dark red) show distinct differences. All of them feature strong absorptions around 250 nm, corresponding to the aromatic polymer backbone.[23] For **2**, an additional absorption at λ_{max} = 384 nm is apparent compared to **P1**. The same absorption is present in the UV/Vis spectrum of 2-ferrocenyl-1,10-phenanthroline (Figure S17) and is thus indicative of its successful incorporation into the precursor polymer. However, it needs to be kept in mind that this absorption is most probably not solely caused by the polymer itself but also by the low molar mass impurity (see Figure S5 and S9). Compared to **2**, a new band at λ_{max} = 568 nm arises in the UV/Vis spectrum of **2-Pd**. This band is neither present in the UV/Vis spectrum of 2-ferrocenyl-1,10-phenanthroline (Figure S17) nor in that of Pd(cod)Cl_2 (Figure S18) and is thus indicative of the formation of a new species.

To get a deeper insight into the nature of the observed transitions, time-dependent density functional theory (TDDFT) calculations[24-26] were performed on the model systems depicted in Figure S25. Singlet vertical excitation energies were calculated for the five lowest energy excitations (Table S7 and Table S8). In the UV/Vis spectrum of SCNP **2** an absorption onset at 570 nm can be observed (Figure S16). This is well reproduced by the quantum chemical calculations with the lowest energy excitation of **I** occurring at 522 nm (Table S7). Inspection of the difference of electron densities between ground state and the state resulting from this excitation reveals that it mainly corresponds to a transfer of electron density from Fe *d*-orbitals to the phenanthroline moiety and *d-d* transitions on Fe (Figure S26).

Contrary, the UV/Vis spectrum of **2-Pd** shows an absorption onset at 705 nm (Figure S16). This redshift is excellently reproduced by the calculations with the lowest energy excitation of **II** occurring at 654 nm (Table S8). In analogy to **I**, inspection of the difference in electron density (Figure S28) between ground and excited state indicates that this excitation again corresponds to a transfer of electron density from Fe *d*-orbitals to the phenanthroline moiety. However, additional, dominant contributions centered on the $PdCl_2$ unit of **II** are evident, corresponding to *d-d* transitions on Pd and transitions involving the *p*-orbitals of Cl. Hence, the redshift in the absorption onset observed for **2-Pd** compared to **2** is indicative of successful Pd functionalization. Including the five lowest energy excitations in the visualization of the difference densities of ground and excited state shows additional contributions of *d-d* transitions on Fe and the phenanthroline moiety for **I** (Figure S27) and **II** (Figure S29).

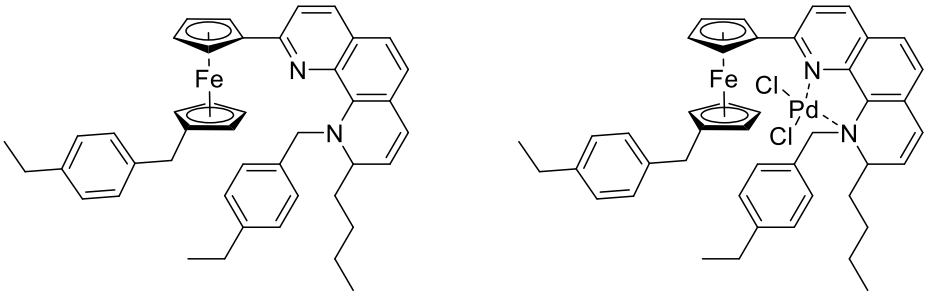

I **II**

Figure S25 Model complexes for the investigation of the optical absorption properties of **2** (**I**) and **2-Pd** (**II**).

Table S7 Five lowest energy singlet vertical excitations (PBE0/dhf-TZVP) of model complex **I**. HOMO – Highest occupied molecular orbital, LUMO – Lowest unoccupied molecular orbital.

	Energy / nm	Oscillator strength / Velocity representation	Contributions (> 10 %)	Orbital pair contribution
1	522.094	0.00112861	HOMO-2 – LUMO+7	23.6
			HOMO-1 – LUMO+7	15.7
			HOMO-1 – LUMO+6	11.7
2	520.832	0.00279587	HOMO-1 – LUMO+7	21.2
			HOMO-2 – LUMO+7	16.4
			HOMO-2 – LUMO+6	13.4
3	476.116	0.00127824	HOMO-5 – LUMO+7	22.5
			HOMO-2 – LUMO+6	14.0
			HOMO-2 – LUMO+5	10.3
4	466.295	0.00006203	HOMO-5 – LUMO+6	16.9
			HOMO-1 – LUMO+6	13.8
			HOMO-1 – LUMO+5	10.0
5	428.740	0.02768946	HOMO – LUMO	96.5

Table S8 Five lowest energy singlet vertical excitations (PBE0/dhf-TZVP) of model complex **II**. HOMO – Highest occupied molecular orbital, LUMO – Lowest unoccupied molecular orbital.

	Energy / nm	Oscillator strength / Velocity representation	Contributions (> 10 %)	Orbital pair contribution
1	653.942	0.00220	HOMO-2 – LUMO	42.7
			HOMO-5 – LUMO	19.3
			HOMO-3 – LUMO	18.7
2	595.030	0.00287	HOMO-3 – LUMO	62.2
			HOMO-5 – LUMO	15.5
3	553.649	0.00040	HOMO-1 – LUMO	26.7
			HOMO-1 – LUMO+2	14.8
			HOMO-1 – LUMO-6	11.4
4	552.695	0.01440	HOMO – LUMO	29.0
			HOMO-5 – LUMO	13.6
5	539.566	0.00688	HOMO-2 – LUMO	16.7
			HOMO-5 – LUMO	16.6

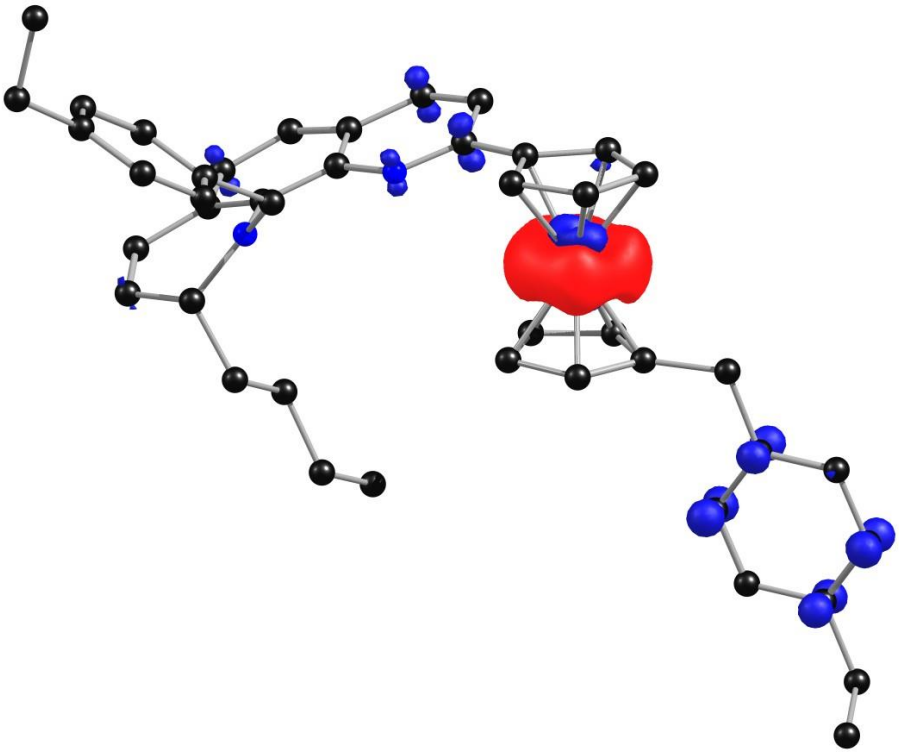

Figure S26 Non-relaxed difference density between the lowest singlet vertical excitation and the ground state of **I** (PBE0/dhf-TZVP). Red color indicates a surplus of electron density for the ground state, blue for the excited state. Contours are drawn at 0.003 atomic units. Hydrogen atoms are omitted for clarity. Carbon black, nitrogen blue, Fe orange.

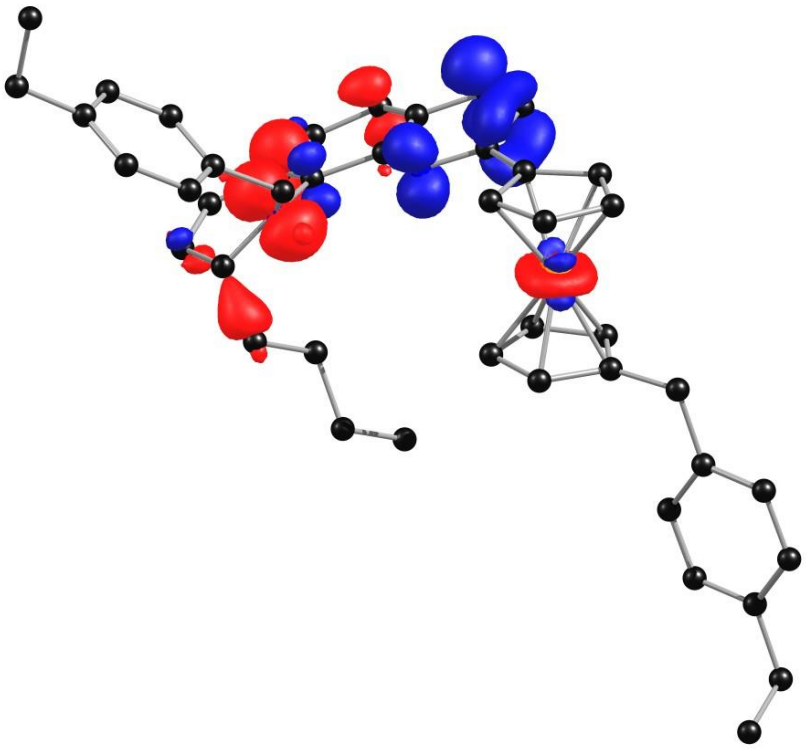

Figure S27 Non-relaxed difference density between the five lowest singlet vertical excitations (weighted by their oscillator stregth) and the ground state of **I** (PBE0/dhf-TZVP). Red color indicates a surplus of electron density for the ground state, blue for the excited state. Contours are drawn at 0.003 atomic units. Hydrogen atoms are omitted for clarity. Carbon black, nitrogen blue, Fe orange.

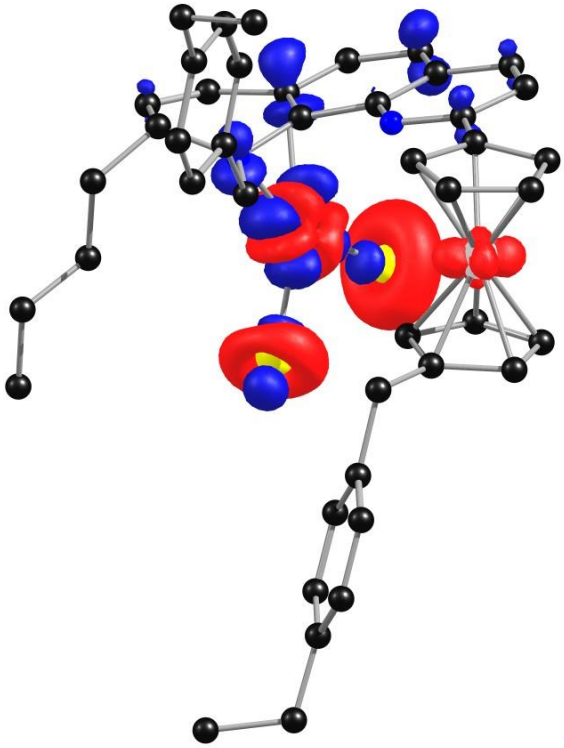

Figure S28 Non-relaxed difference density between the lowest singlet vertical excitation and the ground state of **II** (PBE0/dhf-TZVP). Red color indicates a surplus of electron density for the ground state, blue for the excited state. Contours are drawn at 0.003 atomic units. Hydrogen atoms are omitted for clarity. Carbon black, nitrogen blue, Cl yellow, Fe orange, Pd red.

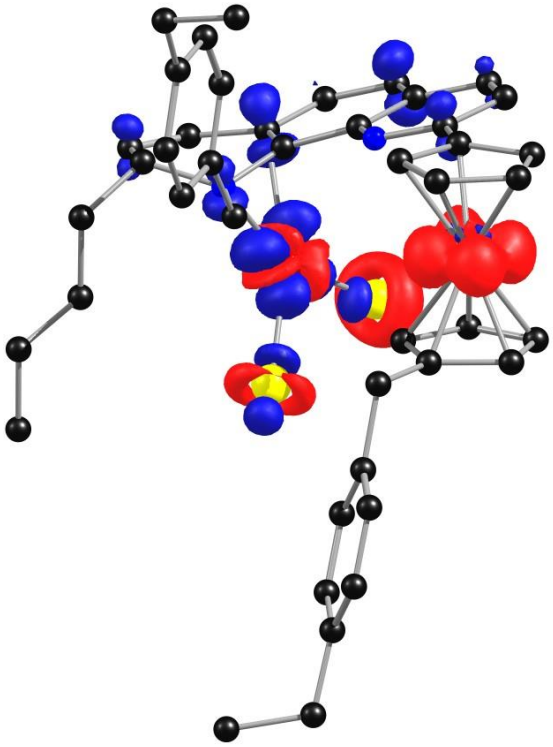

Figure S29 Non-relaxed difference density between the five lowest singlet vertical excitations (weighted by their oscillator stregth) and the ground state of **II** (PBE0/dhf-TZVP). Red color indicates a surplus of electron density for the ground state, blue for the excited state. Contours are drawn at 0.003 atomic units. Hydrogen atoms are omitted for clarity. Carbon black, nitrogen blue, Cl yellow, Fe orange, Pd red.

6 References

[1] N. D. Knöfel, H. Rothfuß, J. Willenbacher, C. Barner-Kowollik and P. W. Roesky, *Angew. Chem. Int. Ed.*, 2017, **56**, 4950.

[2] I. R. Butler and J. L. Roustan, *Can. J. Chem.*, 1990, **68**, 2212.

[3] J. L. Bohlen, B. Kulendran, H. Rothfuß, C. Barner-Kowollik and P. W. Roesky, *Polym. Chem.*, 2021, **12**, 4016.

[4] TURBOMOLE V7.7 2022, a development of University of Karlsruhe and Forschungszentrum Karlsruhe GmbH, 1989–2007, TURBOMOLE GmbH, since 2007.

[5] S. G. Balasubramani, G. P. Chen, S. Coriani, M. Diedenhofen, M. S. Frank, Y. J. Franzke, F. Furche, R. Grotjahn, M. E. Harding, C. Hättig, A. Hellweg, B. Helmich-Paris, C. Holzer, U. Huniar, M. Kaupp, A. Marefat Khah, S. Karbalaei Khani, T. Müller, F. Mack, B. D. Nguyen, S. M. Parker, E. Perlt, D. Rappoport, K. Reiter, S. Roy, M. Rückert, G. Schmitz, M. Sierka, E. Tapavicza, D. P. Tew, C. Van Wüllen, V. K. Voora, F. Weigend, A. Wodyński and J. M. Yu, *J. Chem. Phys.*, 2020, **152**, 184107.

[6] J. P. Perdew, K. Burke and M. Ernzerhof, *Phys. Rev. Lett.*, 1996, **77**, 3865.

[7] C. Adamo and V. Barone, *J. Chem. Phys.*, 1999, **110**, 6158.

[8] F. Weigend, M. Häser, H. Patzelt and R. Ahlrichs, *Chem. Phys. Lett.*, 1998, **294**, 143.

[9] F. Weigend and R. Ahlrichs, *Phys. Chem. Chem. Phys.*, 2005, **7**, 3297.

[10] F. Weigend and A. Baldes, *J. Chem. Phys.*, 2010, **133**, 174102.

[11] K. A. Peterson, *J. Chem. Phys.*, 2007, **126**, 124101.

[12] K. Eichkorn, F. Weigend, O. Treutler and R. Ahlrichs, *Theor. Chem. Acc.*, 1997, **97**, 119.

[13] F.Weigend, *Phys. Chem. Chem. Phys.*, 2006, **8**, 1057.

[14] O. Treutler and R. Ahlrichs, *J. Chem. Phys.*, 1995, **102**, 346.

[15] O. Treutler in Entwicklung und Anwendung von Dichtefunktionalmethoden, Dissertation, Universität Karlsruhe (TH), Karlsruhe, Germany, 1995.

[16] E. Caldeweyher, C. Bannwarth and S. Grimme, *J. Chem. Phys.*, 2017, **147**, 034112.

[17] X. Yang, I. Issac, S. Lebedkin, M. Kühn, F. Weigend, D. Fenske, O. Fuhr and A. Eichhöher, *Chem. Commun.*, 2014, **50**, 11043.

[18] T. Wang, F. Chen, J. Qin, Y. He and Q. Fan, *Angew. Chem. Int. Ed.*, 2013, **52**, 7045.

[19] W. Yang and T. Nakano, *Chem. Commun.*, 2015, **51**, 17269.

[20] O. Moudam, F. Ajamaa, A. Ekouaga, H. Mamlouk, U. Hahn, M. Holler, R. Welter and J. Nierengarten, *Eur. J. Org. Chem.*, 2007, **2007**, 417.

[21] I. R. Butler, *Organometallics*, 1992, **11**, 74.

[22] A. E. Reed, R. B. Weinstock and F. Weinhold, *J. Chem. Phys.,* 1985, **83**, 735.

[23] T. Li, C. L. Zhou and M. Jiang, *Polym. Bull.*, 1991, **25**, 211.

[24] F. Furche and D. Rappoport in Density functional methods for excited states: equilibrium structure and electronic spectra, Computational Photochemistry, edited by M. Olivucci, *Theor. Comput. Chem.*, 2005, **16.**

[25] R. Bauernschmitt and R. Ahlrichs, *Chem. Phys. Lett.*, 1996, **256**, 454.

[26] R. Bauernschmitt, M. Häser, O. Treutler and R. Ahlrichs, *Chem. Phys. Lett.*, 1997, **264**, 573.